PULSED LASER ANNEALING AND CHARACTERIZATION OF GaAs SUBSTRATES

by

YANAN F. SHIEH

B.S., Shanghai University, 1984
Shanghai, P. R. China

A MASTER'S THESIS

submitted in partial fulfillment of the

requirements for the degree

MASTER OF SCIENCE

Department of Electrical and Computer Engineering

KANSAS STATE UNIVERSITY
Manhattan, Kansas

1989

Approved by:

Andrzej Rys

Major Professor

TABLE OF CONTENTS

LIST OF FIGURES

LIST OF TABLES

ACKNOWLEDGMENTS

I wish to express my gratitude to my major professor, Dr. Andrzej Rys, for his advice throughout the research. My thanks also go to Dr. Richard Gallagher and Dr. Kenneth Shultis for being on my committee.

I would like to thank the Department of Electrical and Computer Engineering and my family for providing their support during my graduate program.

I am also grateful to the people in Honeywell and Motorola for their donation of the ion implanted GaAs.

I. INTRODUCTION

The benefits of using semi-insulating gallium arsenide (GaAs) as a substrate material for high performance devices over silicon have been recognized for many years. Moreover, the development of GaAs ICs has lagged behind that of Si ICs since the technology applied on silicon is not very suitable on GaAs. With the great progress in science, silicon ICs are no longer attractive in those areas which demand high speed devices and IC chips. Extensive research of GaAs has been focused on the development of GaAs technology since the beginning of 70's due to the high electron mobility, the high peak electron velocity and the low intrinsic carrier concentration of GaAs material. In recent years, GaAs digital integrated circuits were widely used for high-speed acquisition of very-wide-bandwidth pulsed, pseudo-random or continuous stream data and its processing in real time in military, biomedical research, and communication[1]. With these broad applications, GaAs technology is becoming more and more important for optimization of such devices. So far, there has been great effort made in GaAs material processing, such as the growth of GaAs semi-insulating substrate, epitaxial deposition and ion implantation. Moreover, further research has gone beyond the processing techniques

has been in the area of semiconductor material testing which characterizes deep level defects and electrical properties of processed semiconductors. The methods used successfully to characterize deep levels include the capacitance transient spectroscopy and the current transient spectroscopy for both conductive and high resistivity substrates.

Research work involved in the pulsed laser annealing and characterization of GaAs has been conducted during the past few years by the solid state group in the Department of Electrical and Computer Engineering, Kansas State University. An n-type ion-implanted GaAs was studied after a pulsed laser annealing process. Development of the pulsed laser annealing system with an XeCl excimer laser (λ= 308 nm) in the laser laboratory at KSU was described elsewhere[9].

The contribution of this study towards the long term research project at KSU was in the area of characterization of n-type ion-implanted GaAs. It dealt with deep levels measurements, and depth profiling of electron density and mobility on pulsed laser and conventional furnace annealed samples. Van der Pauw and Hall techniques were introduced to achieve carrier activation and electron mobility. In addition, with the patient help of Mr. Ahkter Ahmed, a photo-induced

transient spectroscopy (PITS) system was developed for deep levels measurements on the n-type GaAs with a semi-insulating substrate.

In this thesis, the main discussions will focus on the characterization of ion-implanted GaAs substrate with different dopant impurities, doses and annealing processes.

1.1 A Description of Gallium Arsenide (GaAs)

Gallium arsenide (GaAs) is a compound semiconductor material. The element gallium (Ga) is from group III, while arsenic (As) is located in group V in the periodic table. By making an alloy of the two above elements at high temperature, a GaAs single crystal can be grown by various techniques. However, the crystal structure of GaAs presents its own feature uniquely, according to the solid state physics theory.

Fig. 1.1 exhibits the crystal structures of GaAs and Si for indicating the differences between compound and element semiconductors. GaAs has a zincblend lattice which contains two different interpenetrating face-center-cubic (fcc) sublattices displaced by one quarter of the distance along a diagonal of the cube. Then each ion, gallium or arsenic, is symmetrically surrounded by four ions of the other element, each lies at a regular tetrahedral. Si, in contrast to GaAs, has two identical interpenetrating

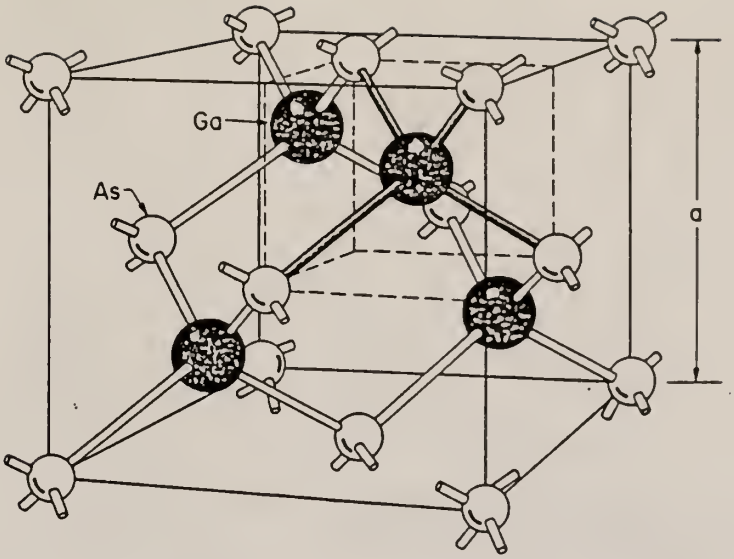

(a) Zincblende Lattice

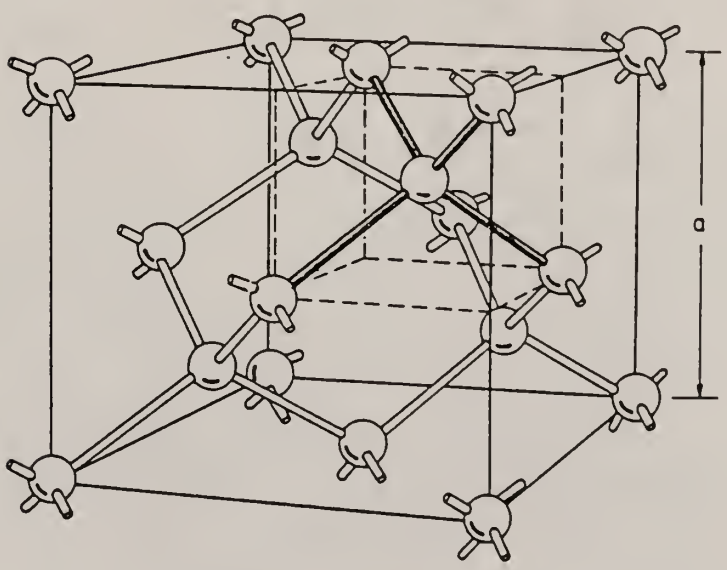

(b) Diamond Structure

Fig. 1.1 Crystal structures of gallium arsenide and silicon.
From S.M.Sze, Semiconductor Devices

face-center-cubic (fcc) sublattices to form a diamond lattice. Therefore, each atom is surrounded by the four nearest silicon atoms in the same fashion. From the lattice configuration of GaAs, it turns out that not only GaAs has covalent bonds but also has weak ionic bonds between Ga^+ and As^- ions. This structural character leads GaAs to become thermally sensitive and structurally imperfect, which results in a creation of gallium and arsenic vacancies in GaAs lattice. So far, several GaAs crystal growth techniques have been introduced to minimize the decomposition of GaAs and crystal imperfection, such as Magnetic Liquid-Encapsulated Czochralski (MLEC) with radiation shielding or vertical heating method[1]. In addition, with advanced epitaxy technology[1], the high quality GaAs layers suitable for applications of

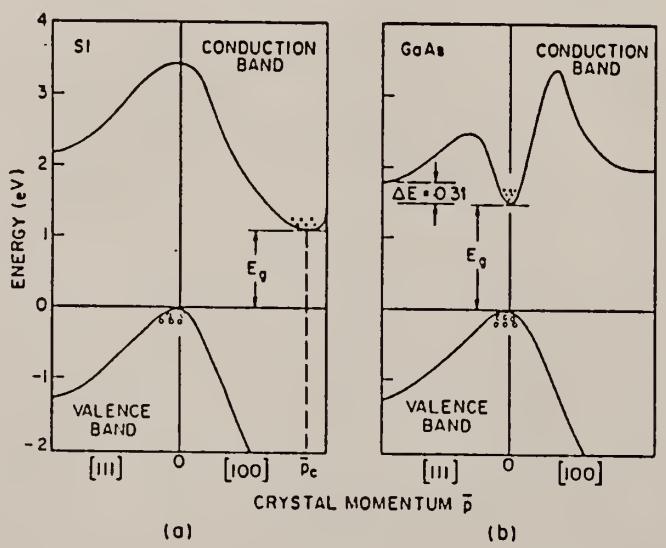

Fig. 1.2 Energy band structures of Si and GaAs From S.M.Sze, Semiconductor Devices

integrated circuits have been achieved on a semi-insulator.

With reference to Fig. 1.2, which shows energy bands for both Si and GaAs, three main differences between Si and GaAs have been observed:

a) The parabola of conduction band in GaAs is sharper than the one in Si.

b) The energy band gap of GaAs is 1.32 eV, which is wider than the energy bandgap of Si. (1.12 eV)

c) GaAs has a direct bandgap structure, i.e. the top of the valence band and bottom of the conduction band are located at the same crystal momentum, while Si has an indirect bandgap structure.

Due to such an energy band structure, GaAs has several attractive advantages which Si does not have. To illustrate these, the following equations of the electron mass and intrinsic density must be introduced[2]

$$m_n = (d^2E_c/dp^2)^{-1} \qquad (1.2.1)$$

$$n_i^2 = (N_c\ N_v)\ \exp[-E_g/2kT] \qquad (1.2.2)$$

where $N_c = 2(2m_nkT)^{3/2}$, is effective density of states in conduction band, $N_v = 2(2m_nkT)^{3/2}$, is effective density of states in valence band, and m_n, m_p are electron and hole effective masses, and p is a crystal momentum. Eq. 1.2.1 illustrates that the electron mass is a function of E_c and

p. Thus, the sharper the parabola, the smaller the m_n will be. This results in high electron mobility and peak velocity because they are inversely proportional to the m_n. The Eq. 1.2.2 shows that the intrinsic carrier density decays exponentially with bandgap E_g. Therefore, the intrinsic carrier density of GaAs is lower than that of Si because of bigger E_g in GaAs. Based on the third observation, it can be noticed that when a transition occurs, an electron jumps from the valence band to the conduction band which requires energy change to overcome the energy gap E_g and also some changes in the crystal momentum for silicon. However, the direct band structure of GaAs, which does not require change of momentum for carrier transition, provides radiative transitions in GaAs material. This property of GaAs has been used for semiconductor laser.

1.2 Annealing Characteristics of Semiconductors

The annealing process is directly related to ion implantation damage, resulting in an amorhpous semiconductor material. Fig. 1.3 illustrates ion implantation damage (also called disorder) formed by a light ion and a heavy ion. Atoms are displaced from their lattice positions due to nuclear collisions of implanted ions. Thus, it will cause a degradation of material

parameters such as carrier mobility and minority carrier life time in semiconductor substrate. Annealing, by means of an appropriate combination of time and temperature, relaxes implanted ions to substitutional sites and replaces atoms into original lattice positions to recover the semiconductor properties.

Annealing characteristics are different with different semiconductor materials. Typically, for a low dose (ion implanted dose <= 5 x 10^{13} cm^{-2}) ion implanted Si substrate, annealing temperature is 800° - 900° C for full recorvery of electrical parameters (n, μ etc.)[3]. In contrast to low dose samples, for a full recovery of high dose (ion implanted dose > 5 x 10^{13} cm^{-2}) ion implanted samples, the annealing temperature increases to 1000° - 1100° C[3]. In the case of GaAs annealing, this becomes more complicated because of certain differences of crystal

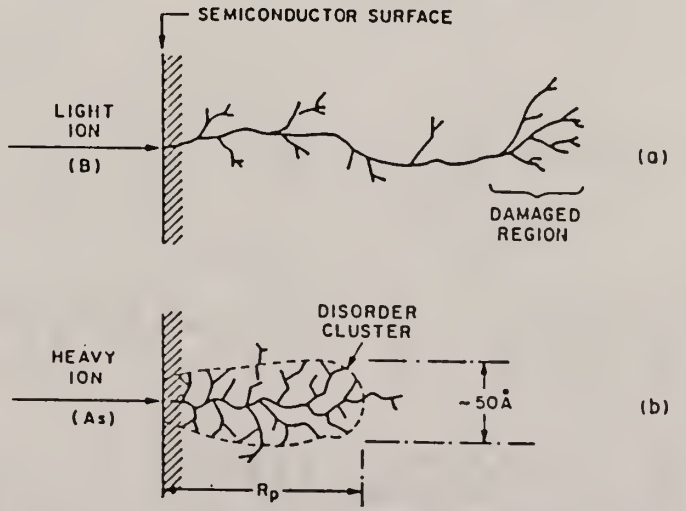

Fig. 1.3 Implantation disorder due to (a) light ions and (b) heavy ions.
From S.M.Sze, Semiconductor Devices

structures between GaAs and Si. Without self-annealing implantation (implantation at elevated temperature), annealing temperature rises to 900°C with 20% recovery for low-dose implantation because it causes movement of two different host species into their appropriate sites[3]. Normally, the annealing temperature stays between 800° - 1100°C for GaAs. Therefore, the decomposition of GaAs surface and arsenic out-diffusion problems are caused by such a high temperature. To minimize these problems, a capping layer like SiO_2 or Si_3N_4 is commonly deposited on the top of the GaAs wafer before ion implantation[3]. But this method adds one extra process to GaAs technology.

The development of annealing technique is related to characteristics of semiconductor materials and applications of semiconductor devices. Furnace annealing, which is simple and easy to perform, is widely used for electron devices processing as a conventional annealing technique. However, with elevated temperature and a time duration, furnace annealing expands impurity depth of ion implantation, which can affect some device paramters. Later, a rapid thermal annealing (RTA), laser annealing and pulsed laser annealing were introduced to overcome the disadvantages of furnace annealing. Rapid thermal annealing provides shorter time (1 - 100 s) and higher temperature than conventional furnace annealing, but it is

still not very suitable for GaAs since decomposition takes place if annealing temperature is above 600° C for any length of time period. The most promising annealing technique in recent years is pulsed laser annealing for device processing of GaAs or other compound semiconductors. It is believed that PLA may allow a cappless annealing which is an important simplification, and may lead to a development of non-alloyed ohmic contacts. A very short time duration when the sample surface is melted by a laser pulse may result in a reduced thermally induced decomposition. Solid state lasers such as Ruby and YAG crystal have been applied in pulsed laser annealing as heating sources[4]. The results indicated several limitations of this technique. The lack of activation in low dosed implanted samples was demonstrated by Shunji Nojima[4] and a residual implantation damage was quoted as the main reason for it. At the same time R. T. Young[5] and her research group examined surface conditions and electrical properties in pulsed Ruby laser annealed samples. A homogeneously annealed surface and an order of magnitude decrease in defect density were observed in Si[5] where an excimer laser light source was used. The attention is focused on annealing n-type ion-implanted GaAs sample with pulsed excimer laser since it causes less defects on the semiconductor substrate. A pulsed laser

annealing (PLA) system with rare gas halide (XeCl) laser was constructed by using a Questek Laser. The goal of this experiment is to examine the effectiveness of pulsed excimer laser annealing in n-GaAs substrate.

1.3 Characterization of Deep Levels in Semi-insulating GaAs

As mentioned earlier, the great potential of semi-insulating GaAs material for high speed devices is recognized. The applications of GaAs devices have gone much further than that of Si devices. However, the fabrication of high speed devices using GaAs has been limited by the material itself. A number of defects present in GaAs material after the crystal growth or the processes used in the fabrication of devices is larger than in Si. Therefore, there has been great effort made to characterize those defects for many years. The earliest work on characterizing deep levels was done by D. V. Lang. The technique introduced by Lang is called Deep Level Transient Spectroscopy (DLTS)[13]. It allows a reliable characterization of deep-level defects. The conventional DLTS technique requires a depletion region or a Shottky barrier in a sample (next to a p-n junction or barrier contact) in which traps are temporarily disturbed as an electrical or optical pulse is applied. By monitoring the

capacitance recovery transient within a depletion layer, capacitance transient spectrum with changing temperature can be recorded. However, it is no longer suitable for semi-insulating (SI) materials since the Debye length $(\kappa\varepsilon_o kT/q^2 n_0)^{1/2}$ is larger than (several mm for SI GaAs at 300 K) dimension of the sample[19]. This means that there is no possibility to form a useful Shottky barrier in the high-resistivity substrate. In 1978, Ch. Hurtes[15] and his team introduced a simple method to characterize deep levels in a high-resistivity GaAs substrate, which was called optical current transient spectroscopy. The sample was irradiated by a laser beam for generating photo-carriers; the transient current was monitored between two contacts on a sample surface. The group concluded that the method gives the same results as conventional DLTS on a conducting layer. The main limitation of the technique is that there is no easy way to obtain the trap concentration.

Due to the difficulty of making the Shottky diode on the laser annealed samples, the conventional DLTS technique failed to work for the samples in this research. Therefore, Photo-induced Transient Spectroscopy (PITS) system was developed by using He-Ne laser pulse instead of an electrical pulse. Fig. 1.4 shows the PITS set-up for the experiment. The other details will be addressed in

section 2.5.

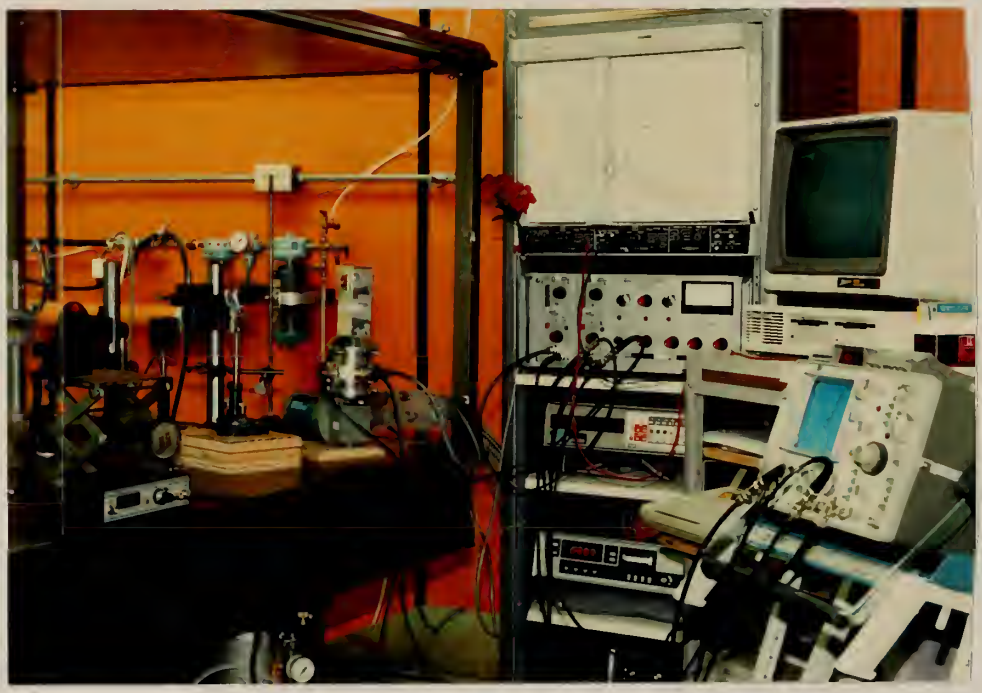

Fig. 1.4 PITS system for characterization of deep-level defects

II. EXPERIMENTAL

2.1 Annealing Performance on Ion Implanted n-type GaAs

A. A General Description of Pulsed Laser Annealing (PLA)

The pulsed laser annealing was accomplished by using a Questek series 2000 excimer laser (λ = 308 nm) along with several external optical equipment to form a uniform excimer laser beam output. The placement of optics involved in this experiment was placed based on an optical system set-up for PLA developed previously (refer to reference 9). Fig. 2.1 shows a block diagram of PLA and its optical set-up along with the names of optics and their relative positions. The purpose of these optical elements explained in reference 9. Six main steps are summarized for this experiment:

[1] Read the Questek Operating Manual to be familiar with the excimer laser. Check XeCl gas pressure and turn on the excimer laser properly.

[2] Set up the optics according to the arrangement in Fig. 2.1 and mount the sample on the sample holder. A paraseal wax is ideal for sample mounting since the sample can be removed from the holder by heating wax at low temperature without damage.

[3] Check output laser beam uniformity across the aperture by placing an exposed photographic paper close to the aperture, and send a single pulse of laser beam. A uniform laser beam should provide a full clover leaf pattern on a photographic paper.

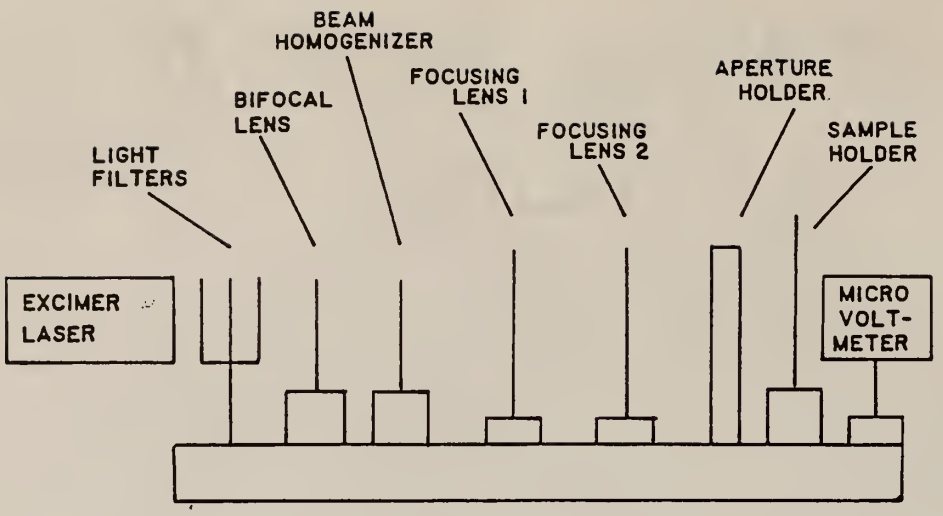

(a)

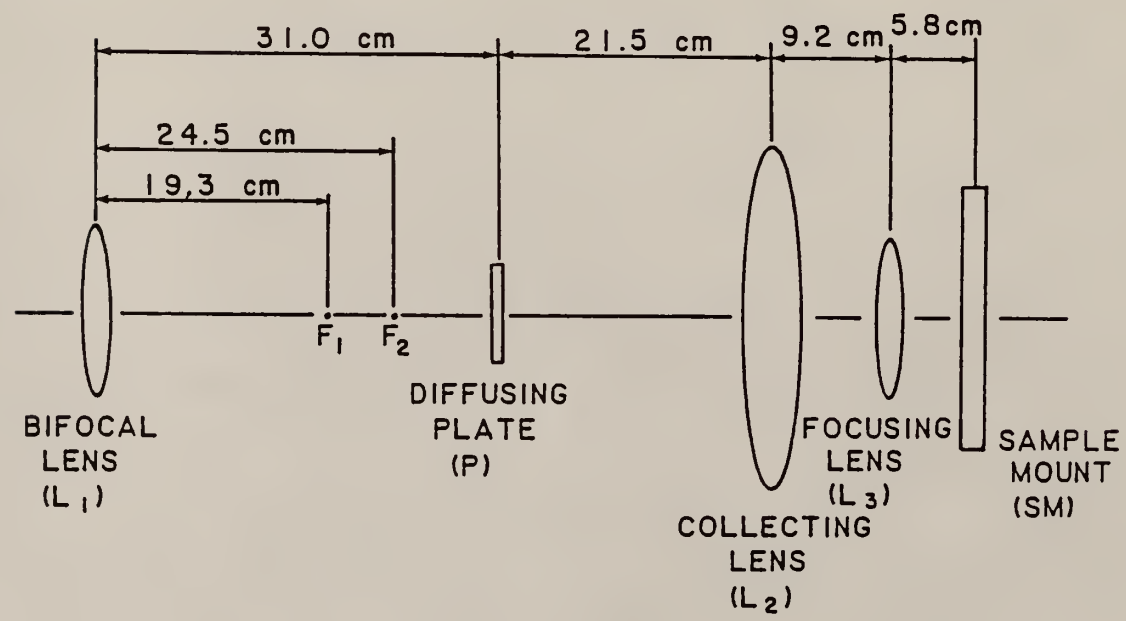

(b)

Fig. 2.1 A block diagram of pulsed laser annealing
(a) outlined set-up (b) optics set-up
From T. W. Chin 9

[4] Check laser intensity across an aperture by using Kiethley 155 null Detector Microvoltmeter. A conversion factor[9] is used for this measurement, i.e. 1 mV is equal to 0.069 Jcm^{-2}.

[5] Insert optical filters to reduce laser intensity if it is necessary.

[6] Open the laser beam latch to let one pulse of laser beam shoot the sample, and close the latch before the next pulse.

B. Furnace Annealing Process

Furnace annealing of ion implanted GaAs samples is less complicated than PLA. The equipment involved in the process are listed as follows:

[a] **Furnace:** provides a high heating system for annealing process.

[b] **Voltmeter:** displays voltage which comes from the thermocouple.

[c] **Thermocouple:** measures the temperature inside the furnace and gives a voltage output.

[d] **Quartz Boat:** drives the sample into the furnace.

The temperature and the time of the FA were approximately 850°C and 20 minutes with 85%N_2 and 15%H_2 (by volume) gas flow. Since FA is a well developed process, it is considered as a reference annealing process. A HP86 computer was connected to the voltmeter to record the annealing temperature during the process. The

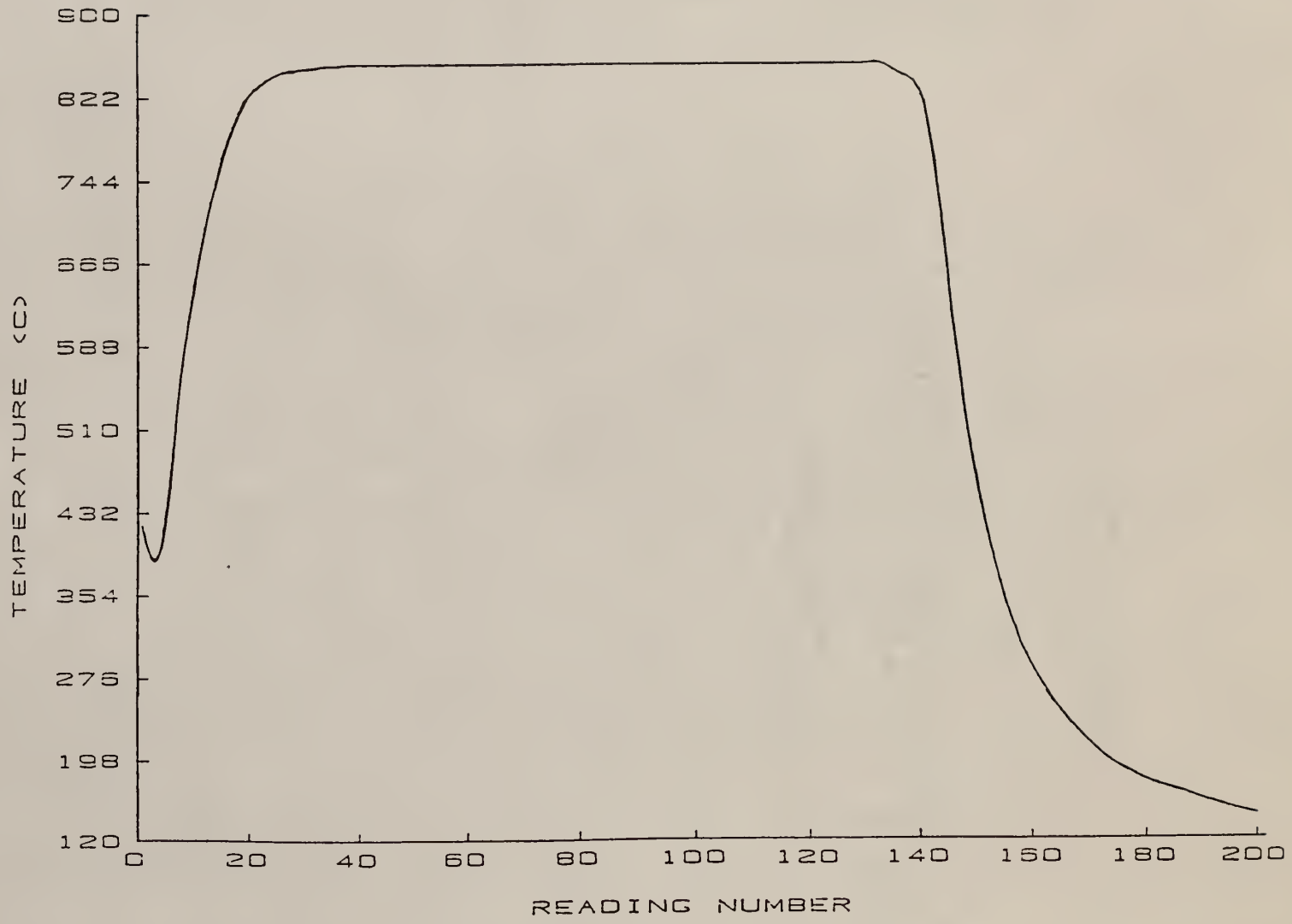

Fig. 2.2 The distribution of temperature in FA process

annealing temperature versus reading number is shown in Fig. 2.2. The set-temperature was 845 C and the maximum temperature was over shooting to 853.8 C. The procedures of FA are simply surmmrized as follows:

[1] Turn on the furnace, 85%N_2 and 15%H_2 by volume, and set annealing temperature. Thereafter, connect HP86 computer, voltmeter and thermocouple. A conversion between temperature and voltage is found in Temperature Measurement Handbook and ENCYCLOPEDIA OMEGA 1985.

[2] Slice two samples of identical size, rinse them with deionized water and dry them using nitrogen gas gun.

[3] Place two annealing samples with face to face, and cover them using two pieces of bulk GaAs, one stays on the top, the other on the bottom, to prevent the out-diffusion of arsenic.

[4] Use quartz tube to push the quartz boat into the furnace. The push-in and pull-out time are about 3 to 5 minutes.

2.2 Measurements of the Electrical Characteristics on n-type GaAs

A. Hall Measurements on a sample with arbitrary shape

Hall measurements are very effective to quantify the number of free carriers. So far, they have been widely used to determine the carrier concentration in doped semiconductor substrates. Hall measurements rely on two external fields, electrical and magnetic. They are applied perpendicularly on a semiconductor sample (see Fig. 2.3).

Then a Lorentz force is generated by the two perpendicular fields. The free electrons will drift toward a direction to balance the Lorentz force (see Fig. 2.3). Eventually an internal electric field called the Hall field is established along the direction of the Lorentz force. In the Hall theory, the Hall effect is represented by measuring a symmetrical semiconductor bar with a known thickness. Under that case, the Hall voltage can be measured directly since there is no net current in the steady state (ab $\perp$ cd). However, the Hall voltage cannot be measured directly if a, b, c, and d are at arbitrary locations. Thus, the static measurements (without nagnetic field) must be taken before a magnetic field is applied. Alternatively, the Hall voltage is expressed as:

$$V_H = V(B) - V(0) \qquad (2.2.1)$$

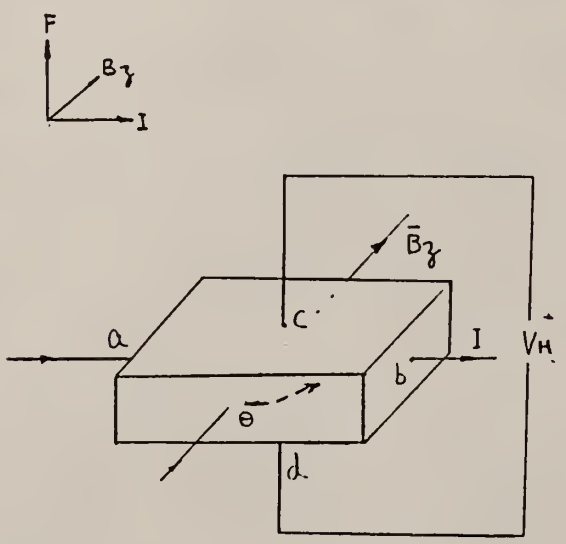

Fig. 2.3 The Hall effect on a symmetrical semiconductor.

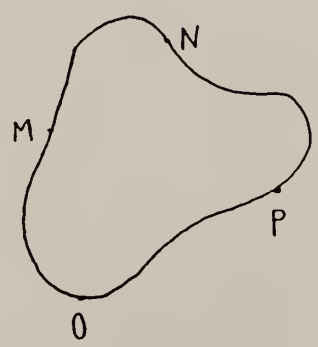

Fig. 2.4 A flat sample of arbitrary shape.

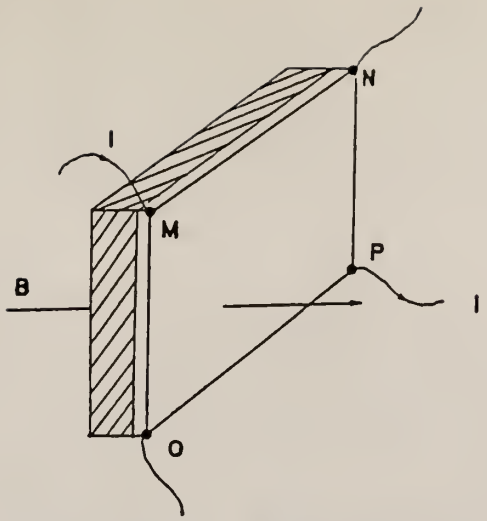

Fig. 2.5 Hall measurements on a FA sample.

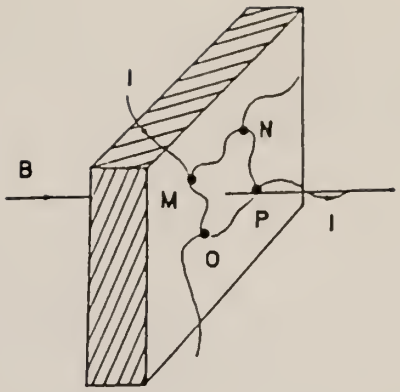

Fig. 2.6 Hall measurement on a PLA sample.

There is only one way to apply the electric and the magnetic fields on the sample (see Figs. 2.5 and 2.6) since the active layer only occupies a part of the substrate. The remaining portion of the substrate is not conductive. Due to a very thin active layer, indium contacts cannot be placed on the side of the sample. Alternatively, the contacts were placed on the surface of the sample. Figs 2.5 and 2.6 show that Hall measurements were carried out for the furnace annealed and laser annealed sample. Once the Hall voltage is known, the carrier concentration can be calculated through the equation derived from the Hall effect[2], i.e.

$$n = \frac{I\ B_z}{q\ V_H\ d} \qquad (2.2.3)$$

where

n = electron carrier concentration in n-type

I = current applied on sample during Hall and van der Pauw measurements

B_z = magnetic field applied in the sample

V_H = Hall voltage

q = charge of electron

d = thickness of sample

In case the thickness of the sample is unknown, the Eq. 2.2.2 is reformed as:

$$n\,d = N_S = (I \cdot B_z)/(q \cdot V_H) \qquad (2.2.3)$$

where N_S = average sheet carrier concentration (cm^{-2}).

B. Van der Pauw Method

Carrier mobility is another electrical parameter that was studied for n-type GaAs. It is expressed as follows:

$$\mu_n = 1/(q \cdot n \cdot \rho) \qquad (2.2.4)$$

where ρ = resistivity of the sample.

The derivation of the Eq. 2.2.4 is shown in reference 2. The carrier concentration n and resistivity ρ both determine the electron mobility μ in the expression above. Thus, resistivity measurements were conducted in addition to Hall measurements. There are several ways to perform resistivity measurements; however, van der Pauw method is

preferred since it has two advantages:

1. There is no sample size limitation as long as contacts are placed peripherally.
2. No surface damage occurs during the measurement.

Four indium contacts M, N, O and P were sintered on the sample. During van der Pauw measurements, one takes two voltage readings between the points M, N and points N, P while a current source is applied to the points O, P and points O, M, respectively. Those two pairs of readings provide two resistances of the sample, $R_{MN,OP}$ and $R_{NP,OM}$, respectively. There is a sample relation between them[10]:

$$\exp(-\pi d/\rho\, R_{MN,OP}) + \exp(-\pi d/\rho\, R_{NP,OM}) = 1 \qquad (2.2.5)$$

where d = thickness of the active layer.

By solving the Eq. 2.2.5[10], the resistivity can be written in the form:

$$\rho = \frac{\pi\, d}{2\, \ln 2} (R_{MN,OP} + R_{NP,OM}) * f_c \qquad (2.2.6)$$

where f_c (a correction factor) is a function only of the ratio $r = R_{MN,OP}/R_{NP,OM}$. The relation between f_c and r is evaluated by means of the complex function derivation[10]. The chart in Fig. 2.7 is a plot of the factor f_c versus ratio r for user's convenience. Alternating the Eq. 2.26, expression of the sheet resistance is obtained as follow:

$$R_S = \frac{\pi}{2\ \ln 2} (R_{MN,OP} + R_{NP,OM})\ f_C \qquad (2.2.7)$$

where R_S = sheet resistance.

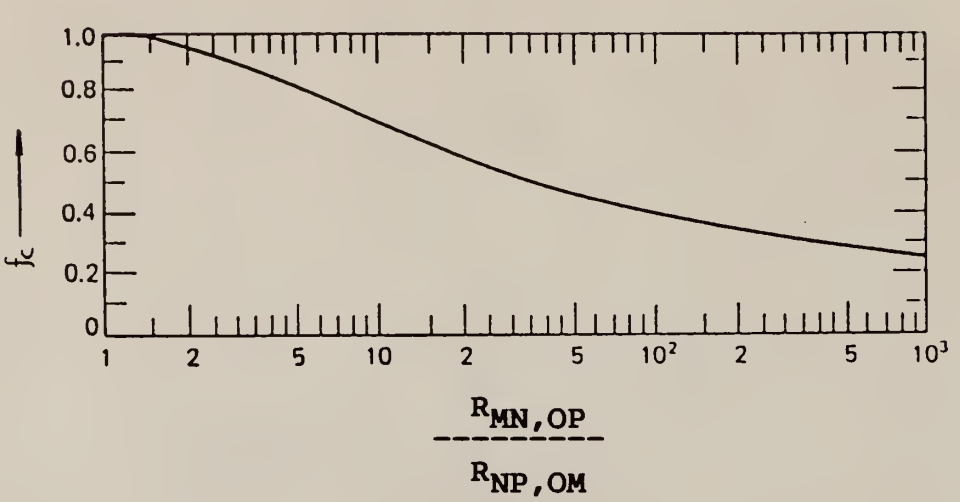

Fig. 2.7 A correction factor for determining specific resistivity.
From Ghandhi, VLSI Fabrication Principles, Si and GaAs

Due to unknown sample thickness, the result turns out to be a sheet resistance in the derivation. Fortunately, the equation for mobility results in proper units(cm^2/V-s) since the sheet carrier concentration in (cm^{-2}) is used

$$N_S = d\ n; \qquad (2.2.8)$$

and

$$R_S = \rho / d; \qquad (2.2.9)$$

then,

$$N_s \cdot R_s = \rho \cdot n; \qquad (2.2.10)$$

The alternative expression of μ_n can be re-written:

$$\mu_n = 1/(N_s \cdot R_s \cdot q) \qquad (2.2.11)$$

2.3 Depth Profiling of Carriers by a Multiple Etching Technique

To observe carrier distribution and variation of carrier mobility of the ion-implanted GaAs after the annealing process, a wet chemical etching method was used successfully to remove a thin layer (~40 nm) at each time on the furnace annealed samples. In this experiment, the selective etchant was a mixture solution of 98% (by weight) sulfuric acid, 30% hydrogen peroxide and deionized water, which is the most commonly used etchant for GaAs. A ternary diagram shows various etching rates of GaAs with different volume ratios of 98%H_2SO_4 and 30%H_2O_2 and H_2O solution at 0°C (see Fig. 2.8). There are four etching surface states (A, B, C, and D) on the diagram. The etching surface becomes cloudy in regions A and B, and mirror-like in regions C and D.

The selected etching rate for depth profiling process was 0.5 μm/min since the active layer of the sample was thin. The volume ratios of the etchant used were H_2SO_4 : H_2O_2 : $8H_2O$ for low dose GaAs and $17H_2SO_4$: $3H_2O_2$: H_2O by

volume for high dose GaAs. An ice bath was used during etching process to maintain the zero degree etching temperature. Silicone glue was on the top of the indium contacts to protect them from being etched by the etchant.

The depth profile mentioned in this thesis determines the carrier concentration and the mobility variation as a function of the depth. Since van der Pauw and Hall

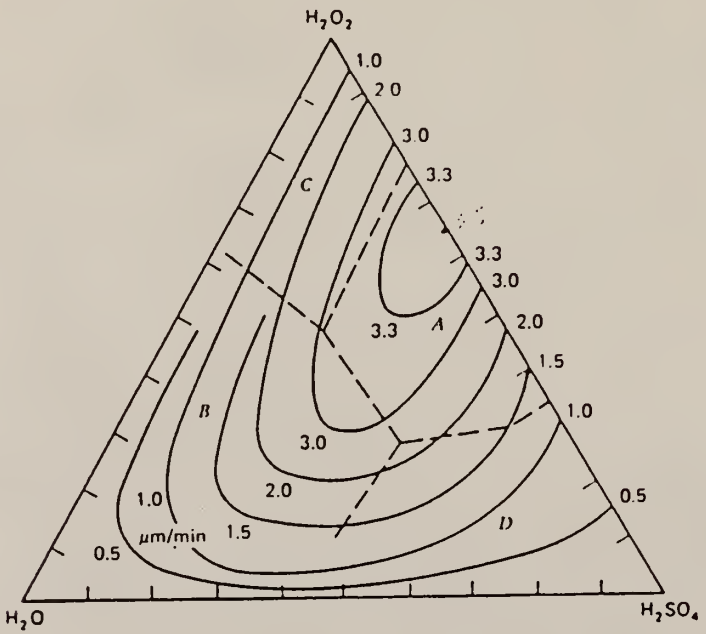

Fig. 2.8 Isoetch curves for GaAs (H_2SO_4 : H_2O_2 : H_2O) system. From Ghandhi 3

measurements provide sheet resistance and sheet Hall coefficient, the effective mobility can be determined from the following relation:

$$\mu_{eff} = H_s/R_s \qquad (2.3.1)$$

where H_s is a sheet Hall coefficient, and

$$N_s = (R_s\, q\, \mu_{eff})^{-1} \qquad (2.3.2)$$

Both μ_{eff} and N_s are weighted averages since the carrier concentration and carrier mobility are depth dependent in an implanted layer. From this point, the Hall coefficient H can be constructed as a summation of the average values of carrier concentration n_i and mobility μ_i in i-th layers of the thickness d_i[11].

$$H = \frac{\sum_i n_i\, \mu_i^2\, d_i}{q(\sum_i \rho_i\, n_i\, \mu_i\, d_i)^2} \qquad (2.3.3)$$

By making the assumption that the Hall mobility is equal to conductivity mobility, the conductivity will be

$$\sigma = (q/d)\sum_i n_i\, \mu_i\, d_i \qquad (2.3.4)$$

in i-th layer since $\mu = 1/(q\, N_s\, R_s)$ in each layer. Then,

$$R_s = (\sigma d)^{-1} = 1/q\sum_i n_i\, \mu_i\, d_i \qquad (2.3.5)$$

where $d = \sum d_i$.

From Eqs. 2.3.3 and 2.3.5, it can be observed that the effective Hall coefficient and sheet resistance are contributed by the carrier concentration and the mobility in each layer. Contrarily, the carrier concentration and the mobility of each layer certainly can be expressed by the two different Hall coefficients and sheet resistances.

They are obtained respectively before and after each

layer is removed. Mayer [1967] reported one method to determine μ_i and n_i from the combination of stripping techniques and Hall measurements. Following Mayer's idea, the carrier concentration by volume in the i-th layer and its mobility are found

$$(H_S)_i/(R_S)_i - (H_S)_{i+1}/(R_S)_{i+1} = q\, n_i\, \mu_i\, d_i \qquad (2.3.6)$$

and

$$(R_S)_i - (R_S)_{i+1} = q\, n_i\, \mu_i\, d_i \qquad (2.3.7)$$

Combining these two equations,

$$\mu_i = \Delta\,(H_S/R_S^2)/(1/R_S)_i \qquad (2.3.8)$$

$$n_i = \Delta\,(1/R_S)_i/(q\, d_i\, \mu_i) \qquad (2.3.9)$$

2.4 Instrumentation and Implantation for Profiling Process

Equipment used to provide the Hall and van der Pauw data on a GaAs sample is listed below:

[1] **Half-inch gap Electro-magnetic System**
generates a magnetic field B; its value is adjusted by varying output voltage on a variac transformer.

[2] **Bell 601 Gaussmeter:**
measures B field within half-inch gap through an equipped external aluminum enclosure probe.

[3] **Current Source Model 110, Lakeshore Cryotronics**
provides a constant electric field on the sample

for both Hall and van der Pauw measurements.

[4] **Multiprobe Model ss12, Solid State Lab KSU**
is constructed specially for the profiling process since the sample needs to be mounted on the probe during the entire profiling process.

[5] **Programmable Digital Multimeter, Fluke 8520A**
takes each potential reading automatically from the sample as the current is varied. It is controlled through the interface by a program written on HP86 computer.

[6] **Hewlett Packard 86 Computer**
loads a program called "AUTO" to operate DVM and to collect data.

The connections among the equipment during the measurements are shown in Fig. 2.9. The multiprobe was taken away from the magnetic field, while only the current was applied to one side of the sample and the voltage was measured on the other side in parallel for van der Pauw measurements.

Depth profiling requires multi-measurement to provide carrier density and mobility within a thin active layer. It would be very time consuming to record the data manually at each time and to evaluate the carrier concentration and mobility of each layer through the Eqs. 2.3.8 and 2.3.9.

For these reasons, a routine "AUTO" was generated to simplify the entire depth profiling process (see Appnedix E). Essentially, rountine "AUTO" consists of three parts:

[1] **Data Measurement** (see AUTO" line 530 to line 600) performs five voltage readings for a measured data on the DVM and records the average value of those readings on the HP86 computer (see Appendix E).

[2] **Parameters Evaluation**

provides the calculations of an average sheet carrier concentration and a carrier mobility; and a carrier concentration and a mobility of the i-th layer based on Eqs. 2.2.3, 2.2.11, 2.3.8, and 2.3.9.

[3] **Carrier Distribution and Mobility Variation Plot**

retrieves $n_i(x)$ and $\mu_i(x)$ from data array and plots them on linear-log plot respectively.

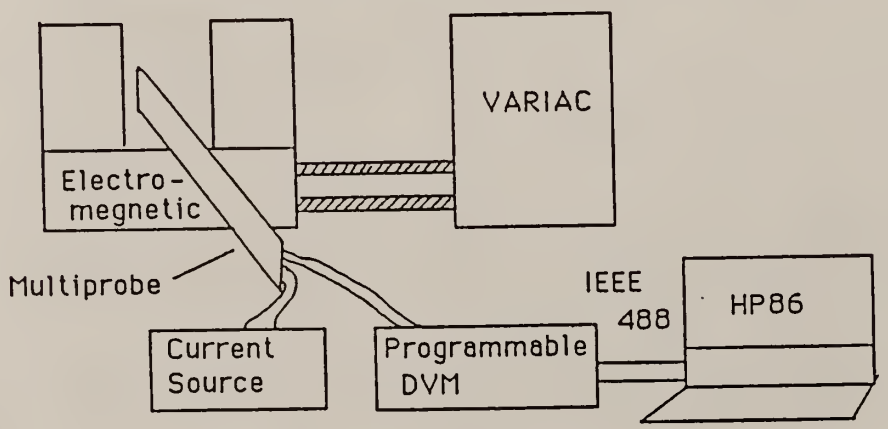

Fig. 2.9 A block diagram of instrumentation for depth profiling measurements

2.5 Photo-Induced Transient Spectroscopy on n-type Ion-Implanted GaAs

A. Derivation of Parameters in Photo-induced Transient Spectroscopy

The parameters which are applied to characterize deep levels in the band gap of a semiconductor are the activation energy, E_t (the energy required to activate the trapped electrons or holes on the deep levels) and the capture cross section σ_n, which relates to the effectiveness of a defect level to capture an electron[2]. In addition, the emission rate will be determined for this scanning-PITS technique.

To facilitate this determination, the energy band diagram of a deep level and its related thermal and optical transient processes are shown in Fig. 2.10 where the superscripts t and o stand for the thermal and optical processes; and c_n, c_p are electron and hole capture coefficients. Note that the arrows indicate the electron transitions. The rate equations for the population of the two trapped carriers in a defect level due to thermal and optical processes are written below:

$$(dn/dt)_T = c_n{}^t np_T - e_n{}^t n_T + c_n{}^o np_T - e_n{}^o n_T \qquad (2.5.1)$$

$$(dp/dt)_T = c_p{}^t pn_T - e_p{}^t p_T + c_p{}^o pn_T - e_p{}^o p_T \qquad (2.5.2)$$

where $(dn/dt)_T$ is the rate of change of electron

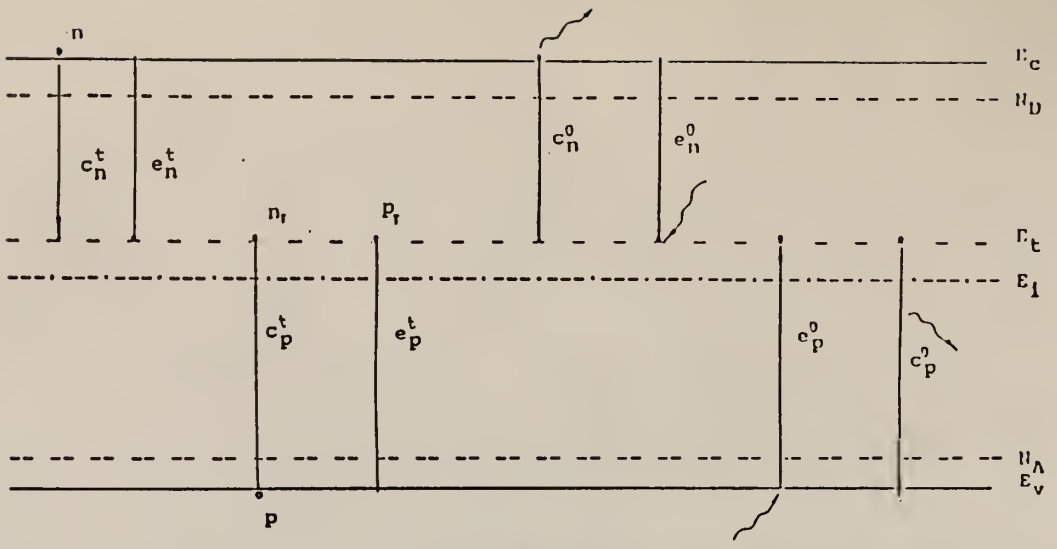

Fig. 2.10 The energy band diagram with the thermal and optical transition processes on a defect level.

concentration of the defect center due to all possible electron transitions between trap levels and conduction band. It is equal to the rate of change of electron density in the conduction band. Similar definition which applies to the transitions of holes between the trap and valence band is denoted by $(dp/dt)_T$. The term (dn_T/dt) denotes the rate of change of total trapped electron concentrationn due to all processes indicated in Fig. 2.10. Then the total change of the trapped electrons as a function of the time on the trap level is

$$\begin{aligned}(dn_T/dt) &= (dn/dt)_T - (dp/dt)_T \\ &= c_n{}^t np_T - e_n{}^t n_T + c_n{}^o np_T - e_n{}^o n_T \\ &\quad - c_p{}^t pn_T + e_p{}^t p_T - c_p{}^o pn_T + e_p{}^o p_T \end{aligned} \quad (2.5.3)$$

By combining the capture and the emission rates of

the thermal and optical processes ($e_n = e_n^t + e_n^o$, $c_n = c_n^t + c_n^o$, etc.) and letting $N_T = n_T + p_T$, which is the total trap density. The Eq. 2.5.3 can be written

$$(dn_T/dt) = -(c_n n + e_n + c_p p + e_p)n_T + (c_n n + e_p)N_T \quad (2.5.4)$$

The general solution of this differential Eq. 2.5.4 is

$$n_T(t) = N_T(c_n n + e_p)/(c_n n + e_n + c_p p + e_p) + C \exp[-(e_n + e_p + c_n n + c_p p)t] \quad (2.5.5)$$

The constant value "C" can be obtained by applying the boundary conditions at $t = 0$ and $t = \infty$ to Eq. 2.5.5.

$$n_T(0) = N_T(c_n n + e_p)/(c_n n + e_n + c_p p + e_p) + C \quad (2.5.6)$$

$$n_T(\infty) = N_T(c_n n + e_p)/(c_n n + e_n + c_p p + e_p) \quad (2.5.7)$$

So,

$$C = n_T(0) - n_T(\infty) \quad (2.5.8)$$

then the $n_T(t)$ can be expressed in terms of $n_T(0)$ and $n_T(\infty)$

$$n_T(t) = n_T(\infty) + [n_T(0) - n_T(\infty)]e^{-t/\tau} \quad (2.5.9)$$

where

$$\tau = 1/(e_n + e_p + c_n n + c_p p) \quad (2.5.10)$$

The expression above is a general case which includes all possible transitions between electrons and holes. It

is fairly complicated. Based on the experimental observation, the expression above can be simplified for the case of an electron (majority carrier) trap. Fig. 2.11 (b) illustrates typical waveforms of PITS measurements observed on the oscilloscope. The entire transient has two parts, rising and decaying transients, which correspond to laser light being on and off, respectively. During the "light-on" period, there is a large number of excess electrons and holes generated in the conduction and valence bands, respectively. The capture process of electrons at the trap level is dominating because of a large concentration of non-equilibrium carriers in the conduction band (the term $c_n n$ is large). The most interesting to us in the PITS experiment is the part of the photo current transient after the light pulse has been turned off. Now, if the direct recombination of electrons between conduction and valence bands is neglected because this process is very fast (in the order of nsec.), the electron emission from the trap would be a dominating process. The capture processes are negligible now, and the expression for τ can be simplified to

$$\tau = 1/e_n \qquad (2.5.12)$$

where τ is the emission coefficient. With these

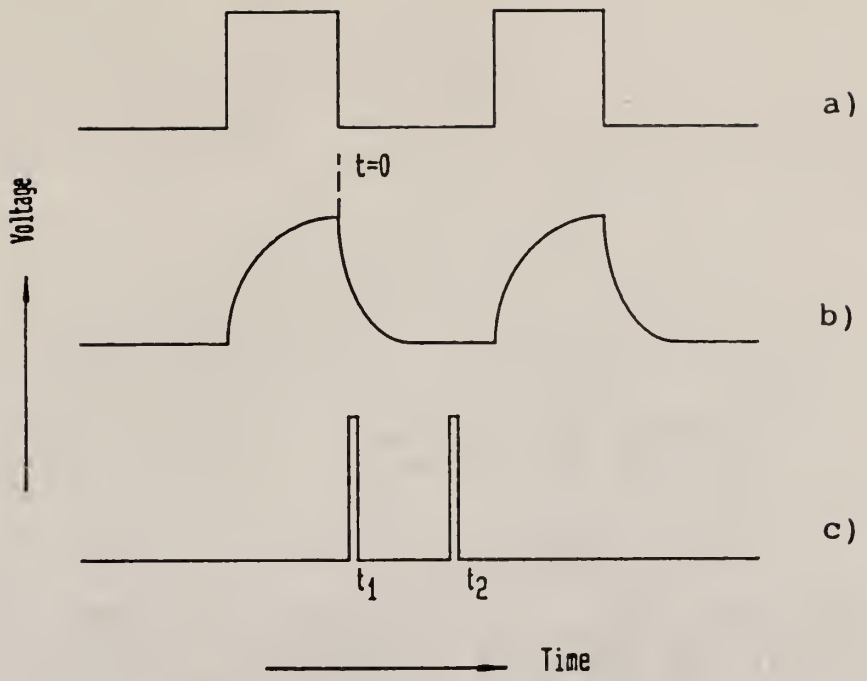

Fig. 2.11 Waveforms for a PITS scan.
a)laser pulse b) PITS transient
c) sampling gates

assumptions, the photo-conductive current generated by electron emission of the traps is[22]

$$i(t) = Ge_n\, n_T(t) = \\ = Ge_n\{n_T(\infty) + [n_T(0) - n_T(\infty)]e^{-e_n t}\} \qquad (2.5.13)$$

and the current difference between the two sampling gates is

$$i(t_1 - t_2) = i(t_1) - i(t_2) \\ = Ge_n N_{TT}(e^{-e_n t_1} - e^{-e_n t_2}) \qquad (2.5.14)$$

where G is associated with electron charge, sample area and penetration depth of the light[22], and N_{TT} is net trap density which participates in the capture and emission

processes for t >= 0. By applying the condition of the maximum i(t) which is $di(t_1 - t_2)/de_n = 0$, the relation between and t_1, t_2 at the temperature T_m in which PITS peak appears can be derived as follows:

$$di(t_1 - t_2)/de_n = GN_{TT}[e^{-e_n t_1} - t_1 e_n e^{-e_n t_1} - e^{-e_n t_2} + e_n t_2 e^{-e_n t_2}] = 0$$

Since $e_n = 1/\tau$, then

$$e^{-t_1/\tau}(t_1/\tau - 1) = e^{-t_2/\tau}(t_2/\tau - 1)$$

$$(t_2 - \tau) = (t_1 - \tau) e^{(t_2 - t_1)/\tau} \qquad (2.5.15)$$

The Eq. 2.5.15 can be solved by a graphical technique[27]. Fig. 2.12 shows the dependence of τ/t_1 versus t_2/t_1. It can be seen that the value of τ/t_1 will approach to 1 when $t_2 >= 8t_1$. In this experiment, the ratio of the t_2/t_1 was kept at 8 which justified the approximation of $\tau \approx t_1$.

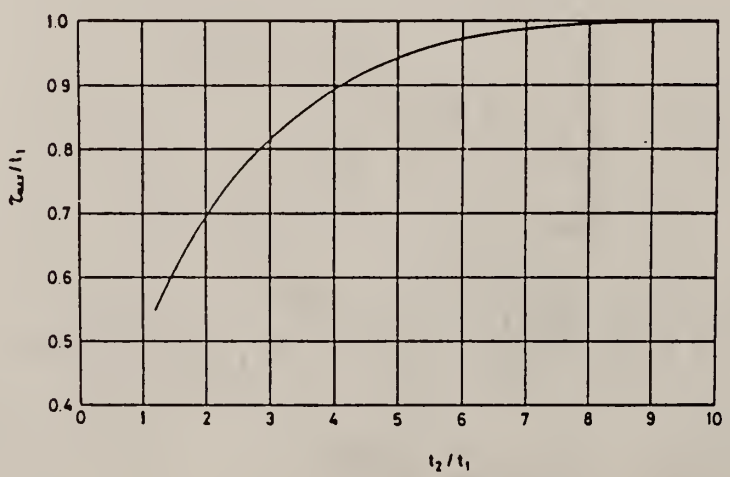

Fig. 2.12 τ/t_1 versus t_2/t_1. From T Itob and H Yanai 27

With respect to the temperature, the recombination process of the electron traps forms the following relation:[2]

$$e_n = 1/\tau = \gamma_n \sigma_n T_m^2 \, e^{-E_t/kT_m} \qquad (2.5.16)$$

$$T_m^2 = (\gamma_n \sigma_n)^{-1} + E_t/kT_m \qquad (2.5.17)$$

By taking natural logarithm to both side of Eq. 2.5.17, it can be re-written

$$\ln(\tau T_m^2) = -\ln(\gamma_n \sigma_n) + E_t/kT_m \qquad (2.5.18)$$

where τ is a material constant, it is 1.9×10^{20} cm^{-2} K^{-2} s^{-1}. Finally the values of E_t and σ_n can be obtained from the slope and intercept of Eq. 2.5.18.

B. Instrumentation and Implementation for Scanning-PITS

A block diagram of scanning-PITS system used for deep level study is shown in Fig. 2.13. This alternative set up in based on earlier capacitance DLTS system. Instead of applying an electrical pulse on the testing sample, PITS introduces an optical pulse to irradiate the sample surface. The optical pulse was obtained by using a 10 mW He-Ne laser (λ= 632 nm along with a motor-driven rotary light-chopper. A 25% optical filter was placed between the laser source and the chopper to cut the beam intensity down to 2.28 mW. The sample was mounted using vacuum

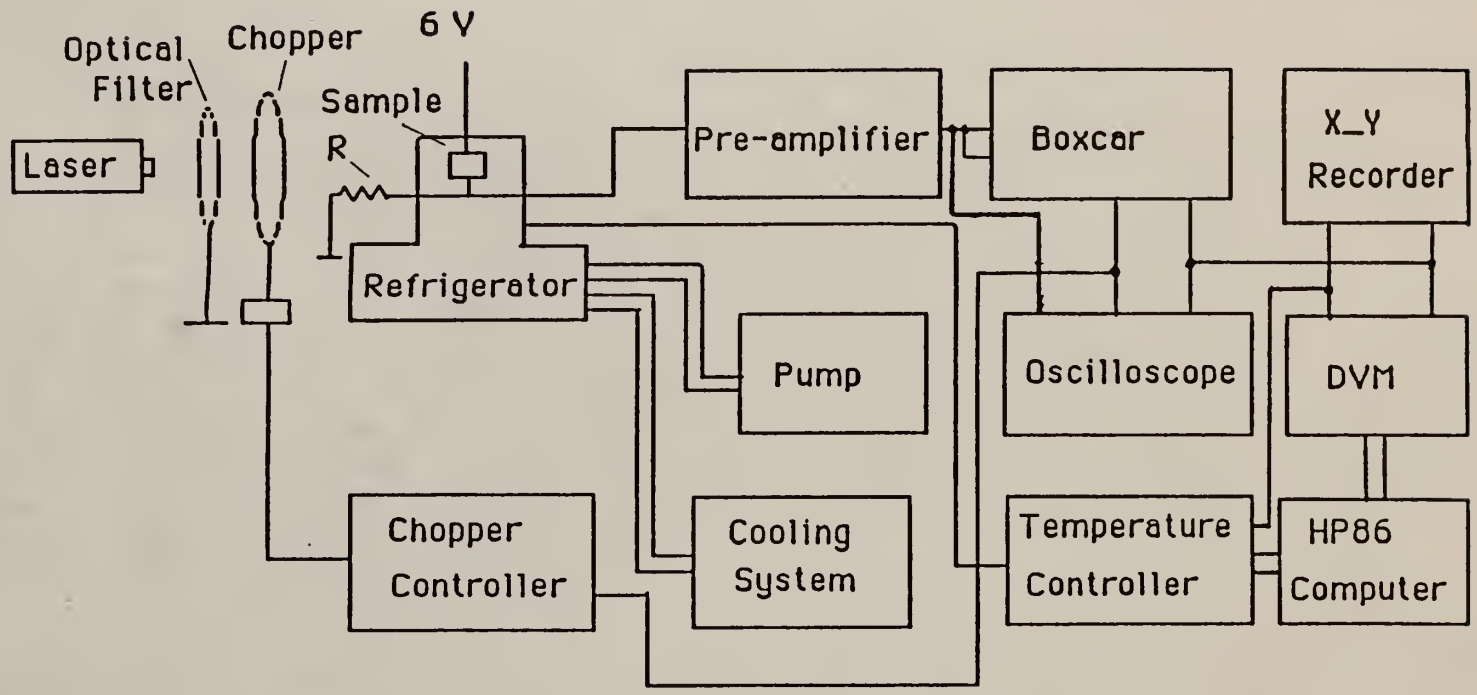

Fig. 2.13 A block diagram of PITS system

grease on a copper block of the second-stage of the closed-cycle helium refrigerator CRYO-TORR 7 cold head[23]. Two thin copper wires for output signal usage were soldered to two indium contacts which were sintered on the sample. A DC bias voltage (6 V) was applied to the sample with a load resistor in series. The transient current was detected as a voltage drop across the load resistor. The temperature was ramped from 40 K up to 380 K during the measurements.

With reference to Fig. 2.13, the applications of the supporting equipment for PITS system are as follows:

[1] **Closed-Cycle Helium Refrigerator**

Model 22 CTI-CRYOGENICS

is connected with cooling system to maintain a low temperature enviroment of the sample.

[2] **Chopper Controller**

Moldel SR540 Stanford Research System, INC.

controls rotating speed of the chopper.

[3] **LOw Noise Pre-amplifier Model 1201 ITHACO**

amplifiers the PITS signal.

[4] **Mechanical Pump**

generates a high vacuum for the enviroment of sample.

[5] **Boxcar Average**

Model 162 EG&G PRINCETON APPLIED RESEARCH

generates sampling gates at the time t_1 and t_2, samples the transient current and takes the difference of two discrete currents as a PITS signal.

[6] **x_y Recorder Model 7045B Hewlett Packard**

is used to record the PITS spectrum.

[7] **Temperature Controller**

Model DRC 81C lake Shore Cryotronics

maintains a set-temperature which is selected by user. For instance, as the temperature falls below the set-temperature, the heater will turn on, otherwise it remains off. It also can be remote-controlled through the interface to ramp temperature up and down gradually.

[8] **Ocsilloscope Hewlett Parckard**

is used to observe the PITS current transient which is shown in Fig. 2.11.

[9] **DVM Model 8520A Fluke**

is remote-controlled to measure PITS signal in volts.

[10] **HP86 Computer**

is used to perform the automatic measurements.

Scanning-PITS measurements were controlled partially by a program called "RAMPING." Therefore, preparations need to be made manually to ensure the accurate PITS

measurements.

1) Adjust the position of the laser spot on the chopper blade until the laser pulse waveform is aligned with the current transient waveform.

2) Align the laser spot with the center of the clover leaf pattern of the sample until the largest PITS signal is observed.

3) Set the position of gate one (t_1) and gate two (t_2) on the boxcar and set-temperature on the temperature controller.

4) Set the "gain" knob of the temperature controller to maximum, and "rate" and "reset" to zero.

5) Once the temperature reaches set-temperature, PITS measurement is ready. then run the "RAMPING".

The implementation of the PITS measurements deals with two things. First, it manages the temperature controller to heat the system with 1-2 K/min heating rate. At the same time it changes the control variables of the heater such as "gain," "rate" and "reset" with an increasing temperature to avoid the temperature oscillation. Secondly, it stores the PITS signal for each set-temperature for plotting the PITS spectrum.

The ramp function is supplied in the temperature controller manual. It ramped the temperature, but did not make a linear temperature ramping. The temperature oscillated in a small range of about 2-3 K or more depending on the power of the refrigerator. As mentioned in the paragraph above, the "RAMPING" (see Appendix E) changes the control variables ("gain," "rate" and "reset")

to minimize the oscillation during a PITS scan. The temperature controller was calibrated manually for each 20 - 30 K to obtain the optimal values of the "gain." ("rate" and "reset" were held at zero. Therefore, the calibrated "gain" values were assigned to the program by means of "if... then" statements. Fig. 2.13 shows the optimized ramping temperature as a function of the time.

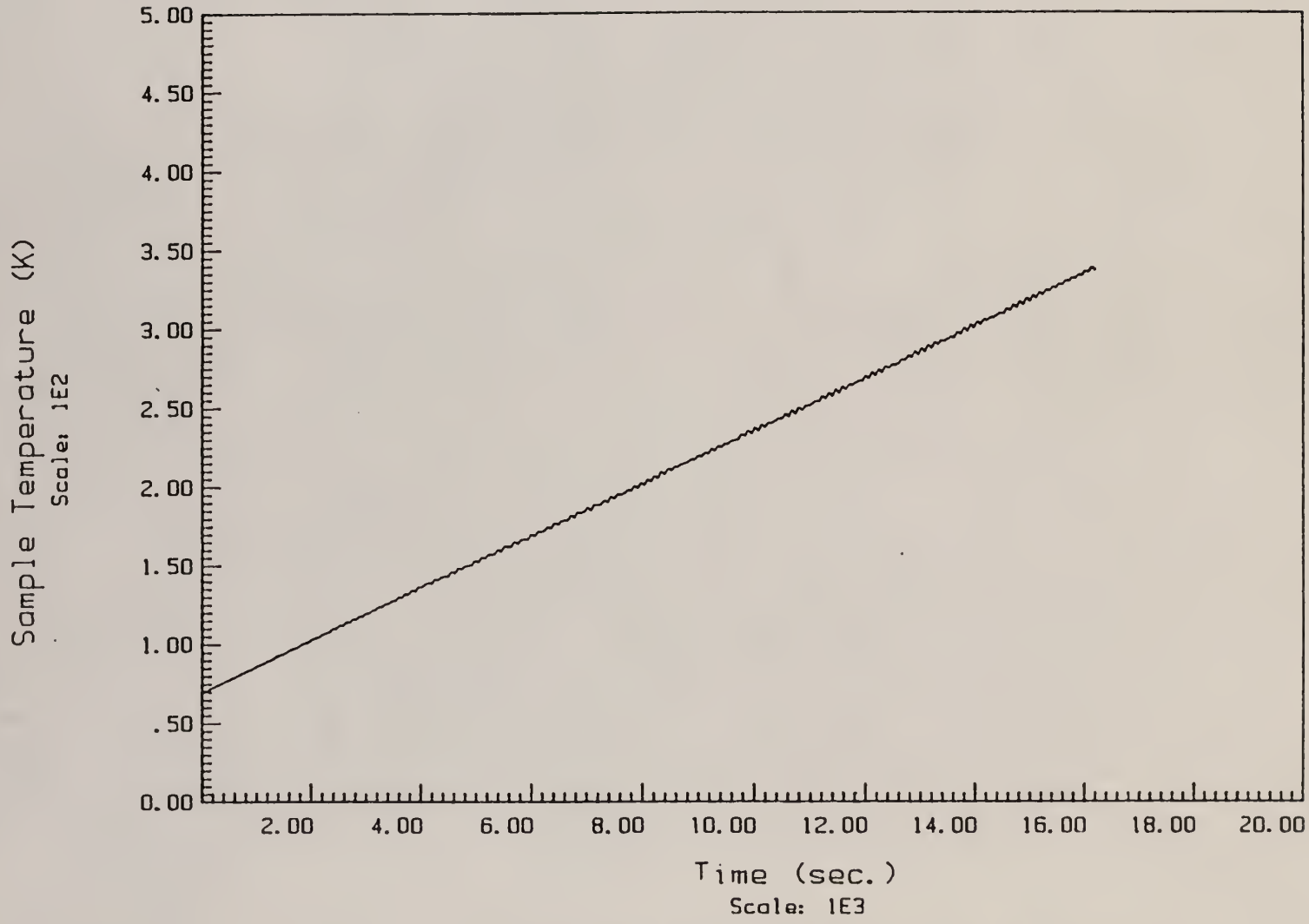

Fig. 2.14 The scanning-PITS temperature as a function of the time.

III. RESULTS AND DISCUSSION

3.1 Electrical Characteristics in Pulsed Laser Annealed GaAs

A. Resistance, carrier activation and electron mobility

Two sets of samples, one of Se implanted GaAs (2.2 x 10^{12} cm^{-2}) annealed with various laser intensities from 0.23 to 0.32 Jcm^{-2} (see Table 3.1a), and the other set of Si implanted GaAs with different doses (from 4 x 10^{12} to 6 x 10^{14} cm^{-2}) but annealed at a constant laser intensity of 0.32 Jcm^{-2} (Table 3.1b) were characterized to reveal their electrical properties, such as resistance, carrier concentration and carrier mobility. From the data presented in Table 3.1a, the following observations can be made

a) The sheet carrier concentration, as measured by a Hall effect, exceeds the dose of implanted impurities. This difference is most pronounced in the lightly doped samples. It is believed that the additional impurity was driven into the substrate from Si_3N_4 by the laser beam since the samples were coated by the nitride cap during the PLA during the PLA process.

b) Electron mobility and sheet carrier concentration increase with the laser intensity. The light

intensity of about 0.32 Jcm^{-2} is the optimum for excimer laser as determined by Raman spectroscopy on a large number of samples[26].

c) It had been observed under the microscope that the annealed surface of the sample with 0.30 Jcm^{-2} laser intensity was inhomogeneous and cloudy. Its mobility and sheet carrier concentration were the lowest, which indicates that the surface morphology can affect greatly the electrical properties of semiconductors.

A few of the Si-GaAs samples were annealed with the excimer laser over a narrow energy range (0.32 Jcm^{-2}) which the previous[11] measurements indicated might be optimum for the highest carrier activation and which had a good mirror-like surface. Table 3.1b lists the results of the PLA Si-GaAs with 0.32 Jcm^{-2} laser intensity.

From Table 3.1b, it is seen that carrier activation exceeds the doping density in low dose samples. In contrast to low dose samples, carrier activation is quite reasonable in high dose samples, especially in 1.0×10^{14} cm^{-2} sample where 83% of implanted impurities are electrically active. The sheet carrier concentration, as determined by Hall effect measurements, is approximately the same for all samples studied at light intensity of 0.32 Jcm^{-2}. The change in electron mobility is not

Table 3.1a Electrical properties of PLA Se-GaAs (2.2 e12 cm-2) with various laser energy.

Laser Intensity (Jcm^{-2})	Sheet Resistance (ohm)	Sheet Carrier Concentration (Jcm^{-2})	Electron Mobility ($cm^{-2}/V-s$)
* 0.23	580	7.1×10^{13}	140
* 0.29	320	7.6×10^{13}	255
0.30	660	7.1×10^{13}	130
* 0.32	254	9.1×10^{13}	270

* Sample used in profiling experiment.

Table 3.1b Electrical properties of PLA (0.32 Jcm^{-2}) Si-GaAs with different doses.

Sample Dose (cm^{-2})	Sheet Resistance (ohm)	Sheet Carrier Concentration (Jcm^{-2})	Electron Mobility ($cm^{-2}/V-s$)
4.0×10^{12}	218	1.1×10^{14}	250
2.0×10^{13}	205	1.0×10^{13}	280
1.0×10^{14}	265	8.3×10^{13}	280
6.0×10^{14}	210	1.0×10^{14}	290

significant, either. This is an indication that the most of the electrically active donors are Si atoms which were diffused in the semiconductor from the Si_3N_4 layer during the pulsed laser annealing. Nojima et. al.[4] reported that

the sample (Si ion-implanted GaAs with 1 x 10^{15} cm^{-2}) annealed by pulsed Ruby laser at 0.79 Jcm^{-2} without nitride cap had an average mobility of 450 $cm^2/V\text{-}s$, and carrier concentration was high (~ 3 x 10^{18} cm^{-3}) in the vicinity of the sample surface (0.4 μm). Referring to the depth profiling performed on Se-GaAs (2.2 x 10^{12} cm^2, see Fig. 3.1) with a laser light intensity of 0.29 Jcm^{-2} in section 3.2, can be noticed that the carrier concentration exceeds 1 x 10^{19} cm^{-3} near the surface (~ 40 nm) which results in a lower mobility of about 250 $cm^2/V\text{-}s$. As discussed discussed earlier, the PLA introduced some amount of impurities into low dose samples from the nitride cap which caused the sheet electron concentration to exceed the implanted fluence of donors, but this did not happen in high dose Si-GaAs samples. This does not eliminate the possibility that impurities are introduced from the Si_3N_4 cap into high doped samples, but the amount is small compared with implanted impurity dose. The diffusion flux of Si atoms during a molten phase of GaAs is smaller in this case because of a large concentration of Si atoms in the substrate, which causes the gradient to be small. It is assumed that the temperature and time are comparable in low and high dose samples for the same laser energy intensity, which would make the diffusivity of Si a constant in both cases.

B. Depth Profiling in PLA Se-GaAs.

Since samples studied in the course of the depth profiling experiment were Se implanted at 320 keV doped to a fluence of $\Phi = 2.2 \times 10^{12}$ cm^{-2} Se during processing, a standard carrier distribution (LSS profile with dash lines)[2] can be obtained from calculations of the projected range (R_p) and standard deviation (ΔR_p). These two parameters can be found once the implanted energy and dose are known. Thus, the carrier density as a function of distance (x) can be expressed

$$N(x) = \frac{\phi}{\sqrt{2\pi} \cdot \Delta R_p} \exp\left[-\frac{1}{2} \left[\frac{x - R_p}{\Delta R_p} \right]^2 \right].$$

The samples used in the depth profiling expriment were marked in Table 3.1a with an asterisk *. The sample annealed under 0.23 Jcm^{-2}light intensity failed completely in this study since there was no activation measured after one etching step (20 nm layer removed). Therefore, no carrier distribution can be obtained by the etching process because the increments ΔH_s and ΔR_s (Eqs. 2.3.8 and 2.3.9) could not be calculated. The active layer was extremely thin (< 20 nm) which resulted in a low mobility probably due to high rate of surface scattering. The carrier distributions of the other two PLA Se-GaAs samples at 0.29 and 0.32 Jcm^{-2} laser intensities are shown in Fig.

3.1. The active layers of these samples were 20 nm and 40 nm, respectively, which were much shallower than the projected range (R_p). It can be seen that the carrier concentration exceeds the impurity density of the theoretical LSS profile in Fig. 3.1.

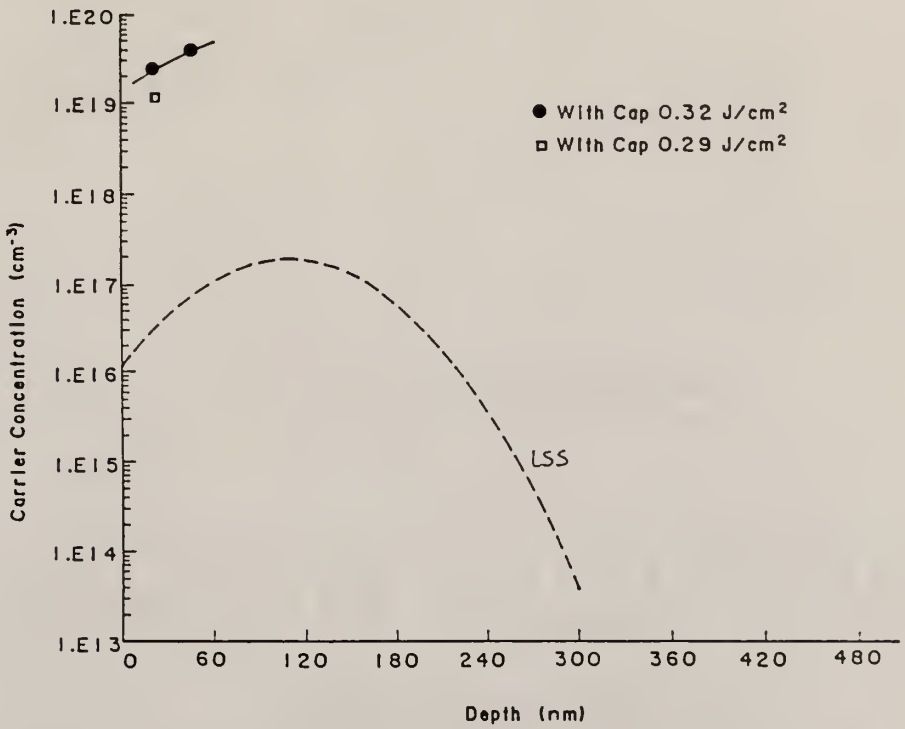

Fig. 3.1 **Carrier distributions of PLA Se-GaAs (2.2 el2 cm-2). The LSS theoretical impurity distribution is shown by a dashed line.**

3.2 Defect Levels and PITS Spectra on n-type GaAs

A. Discussion of defects in PLA and FA GaAs

Before discussing the results of PITS measurements, the names of the tested samples listed in Table 3.2 must be

defined

L2212 = PLA Se-GaAs 2.2×10^{12} cm^{-2}

F2212 = FA Se-GaAs 2.2×10^{12} cm^{-2}

L4012 = PLA Si-GaAs 4.0×10^{12} cm^{-2}

F4012 = FA Si-GaAs 4.0×10^{12} cm^{-2}

L2013 = PLA Si-GaAs 2.0×10^{13} cm^{-2}

L1014 = PLA Si-GaAs 1.0×10^{14} cm^{-2}

L6014 = PLA Si-GaAs 6.0×10^{14} cm^{-2}

F6014 = FA Si-GaAs 6.0×10^{14} cm^{-2}

The eight samples listed above were characterized and their trap levels were revealed by means of photo-induced transient spectroscopy technique. Table 3.2 contains the activation energy (E_t), capture cross section (σ_n), and the peak temperature (T_m) for each trap of all the samples. The labels P_1 through P_5 correspond to the peaks recorded on PITS spectra for all the samples. Fig. 3.2 through Fig. 3.5 show PITS spectra of the eight samples listed above. There are three distinct peaks P_1, P_2, and P_3 present in the laser annealed samples, and three peaks P_1, P_2 and P_4in the furnace annealed samples. They correspond to the defects with the activation energy of ~0.05 eV, 0.1 eV, 0.3 eV and 0.56 eV, respectively. The spectra for highly doped samples (1×10^{14} and 6×10^{14} cm^{-2}), both laser and furnace annealed indicate the presence of an additional peak "P_5" above the room

Table 3.2 Results of defect characterization

Peak	T_m(K)	E_t(eV)	σ_n(cm^2)	Identity	Sample
P_1	48	0.06	1.6×10^{-14}	--	L6014
	57	0.02	2.0×10^{-19}	--	F4012
	58	0.07	2.7×10^{-15}	--	L1014
	60	0.05	3.2×10^{-17}	--	L2013
	62	0.03	3.8×10^{-19}	--	L2212
	70	0.06	1.0×10^{-16}	--	F2212
P_2	83	0.08	1.5×10^{-16}	--	L1014
	83	0.09	8.9×10^{-16}	--	L2013
	86	0.09	2.3×10^{-16}	--	L4012
	86	0.10	1.2×10^{-15}	--	L6014
	87	imprecise	3.5×10^{-20}	--	L2212
	94	0.11	1.5×10^{-15}	--	F6014
	107	0.05	4.3×10^{-19}	--	F4012
	108	0.15	1.0×10^{-14}	--	F2212
P_3	173	0.33	3.1×10^{-12}	EL6	L2212
	175	0.27	5.0×10^{-14}	EL8	L1014
	175	0.23	1.9×10^{-19}	~EL6	L6014
	180	0.25	4.5×10^{-15}	~EL6	L4012
	180	0.32	4.6×10^{-13}	~EL6	L2013
P_4	246	0.32	9.7×10^{-16}	~EL6	F2212
	269	0.30	1.4×10^{-16}	~EL7	F6014
	273	0.56	4.9×10^{-12}	implanted damage	F4012
	279	0.60	1.4×10^{-11}	EL3	F4012
P_5	346	0.80	7.0×10^{-11}	heavily implanted damage	L1014
	357	0.79	1.7×10^{-11}		F6014

~ the level is close to well defined seep level.

-- is not defined.

* τ range: (1.5×10^{-4}, 1.25×10^{3}),

and all E_t inaccuracy: (+/-8% -- +/-10%)

temperature. Due to the weak signal and broad shape of peak "P_5," it was difficult to resolve it accurately (see Appendix C). The activation energy of deep level corresponding to this peak is at approximately 0.80 ev with a capture cross section of about 10^{11} cm^{-2}. This defect level was probably induced by pulsed laser annealing[16], or it may be related to the EL2 defect observed in semi-insulating GaAs substrates grown by LEC (Liquid Encapsulated Czochralski) method without chromium compensation. The EL2 level is generally observed at the temperature of about 390 K.

The next major peak, P_4, appears in the temperature range of 250 - 280 K on PITS spectra of furnace annealed (FA) samples (see Fig. 3.2b, Fig. 3.3b and Fig. 3.4b). For the F4012 sample (Fig. 3.2b), the P_4 is broad and is a result of two seperate but closely spaced defects with activation energies of 0.56 eV and 0.60 eV. The trap at 0.56 eV was found in a Si doped SI GaAs substrate after FA or RTA process and was defined as an ion implantation damage[14]. The trap at 0.60 eV resembles the level called EL3 by G. M. Martin et. al.[18] PITS spectra for the other two FA samples showed a very broad peak within 250 - 280 K range, which was difficult to resolve. The estimate of the activation energies corresponding to this P_4 gave a value of about 0.3 eV for both F6014 and F2212 samples (see

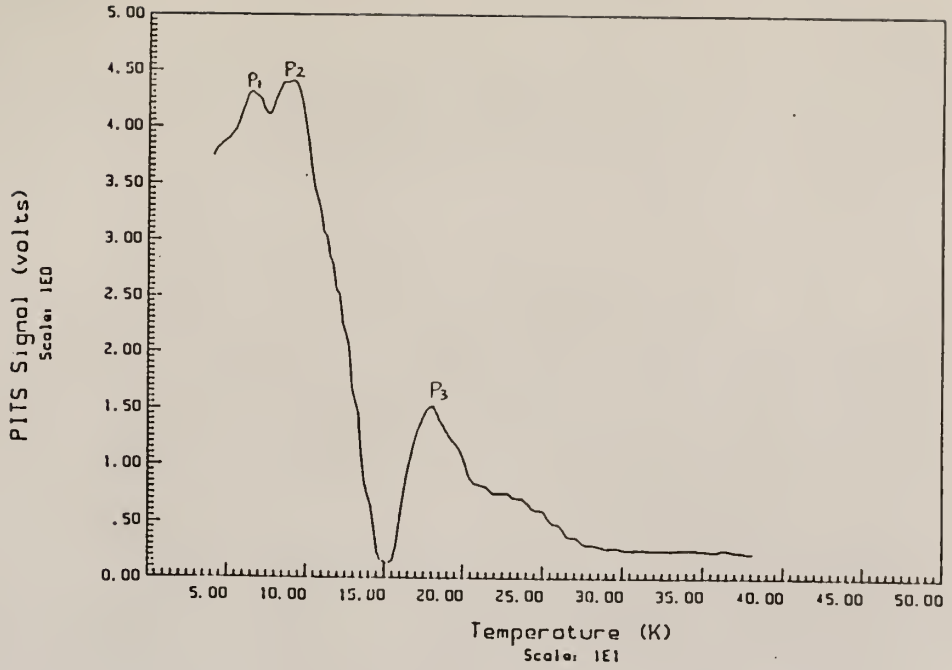

(a)

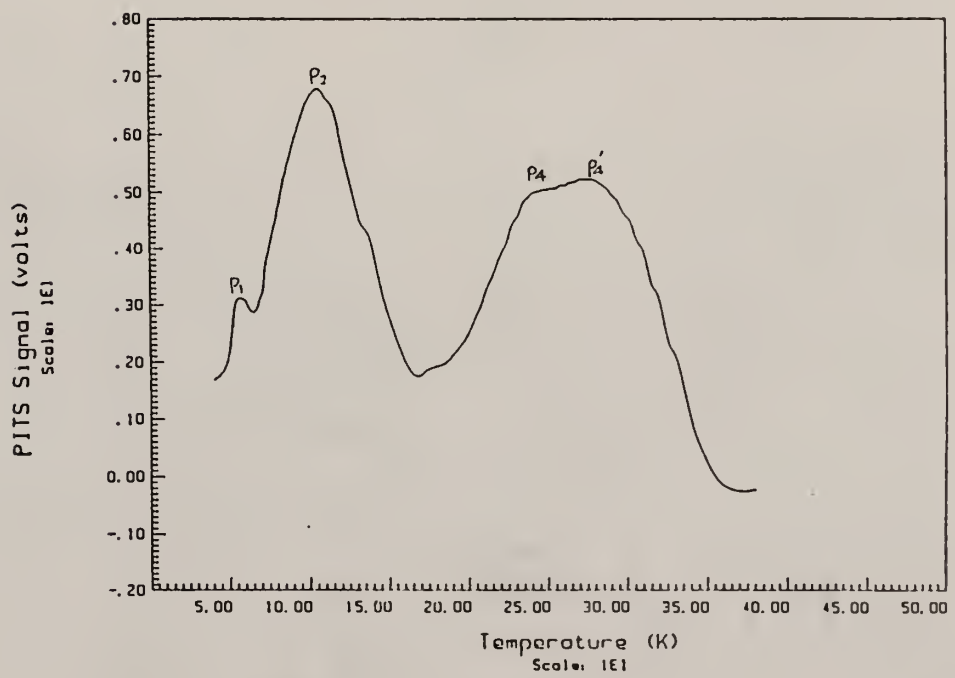

(b)

Fig. 3.2 PITS spectra of Si-GaAs (4.0 x 10^{12} cm^{-2}) at t_1 = 0.3 ms and t_2 = 2.4 ms
a) PLA (I=0.32 Jcm-2) sample b) FA sample

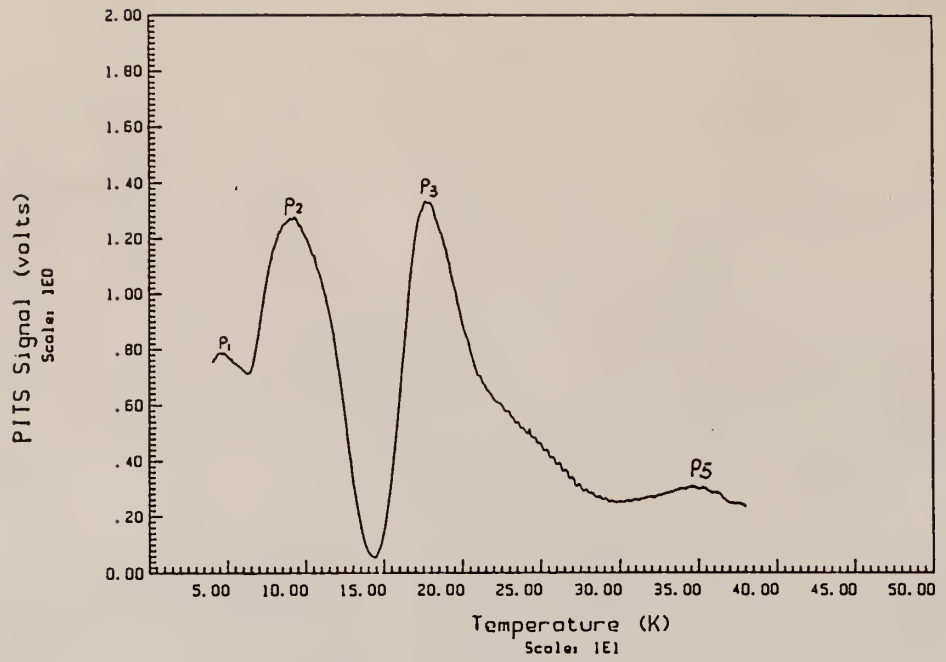

(a)

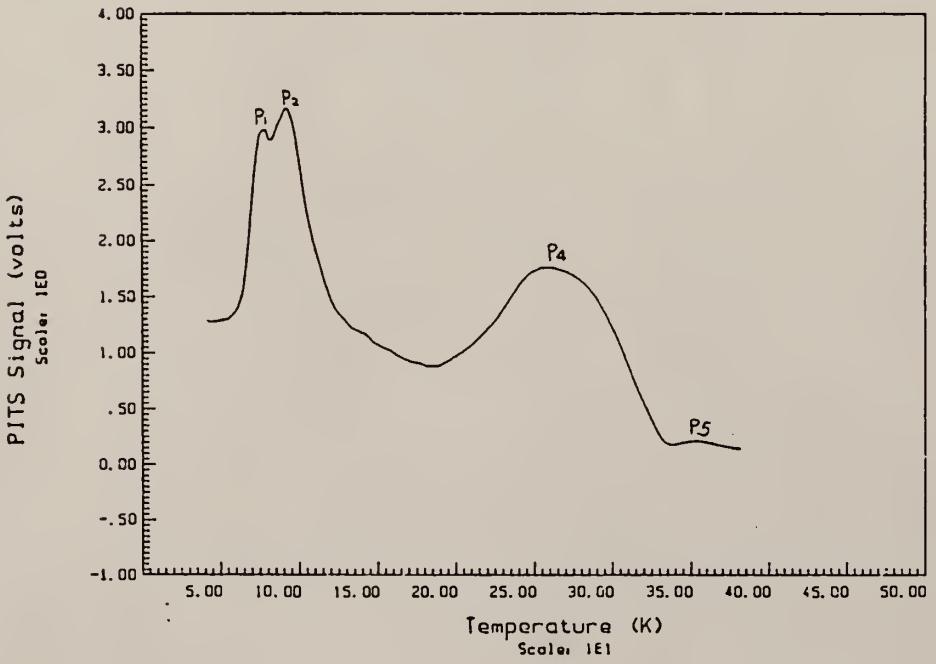

(b)

Fig. 3.3 PITS spectra of Si-GaAs (6.0×10^{14} cm^{-2}) at t_1 = 0.3 ms and t_2 = 2.4 ms
a) PLA (I=0.32 Jcm-2) sample b) FA sample

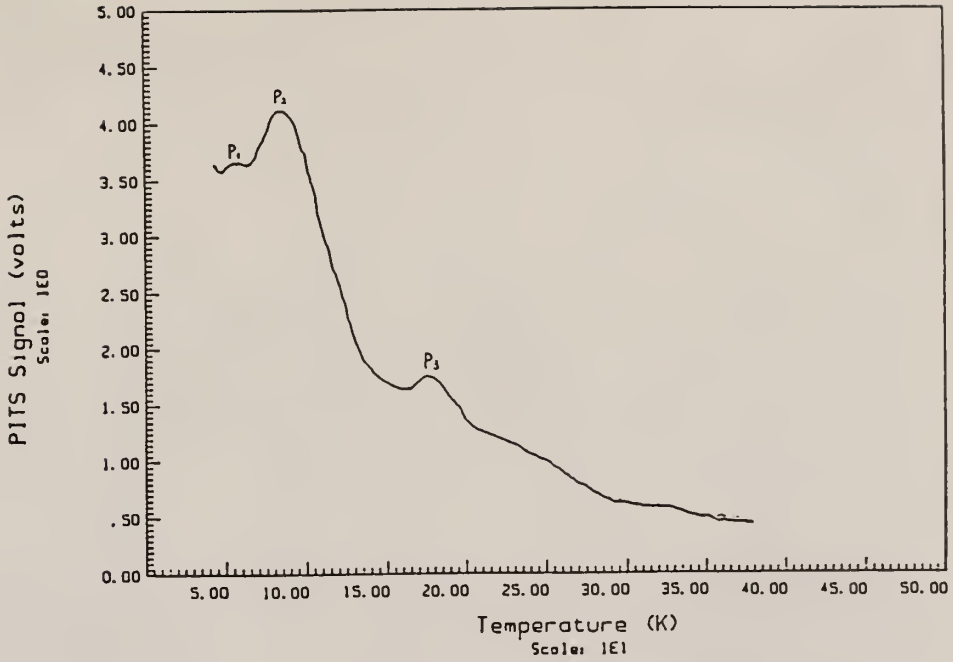

(a)

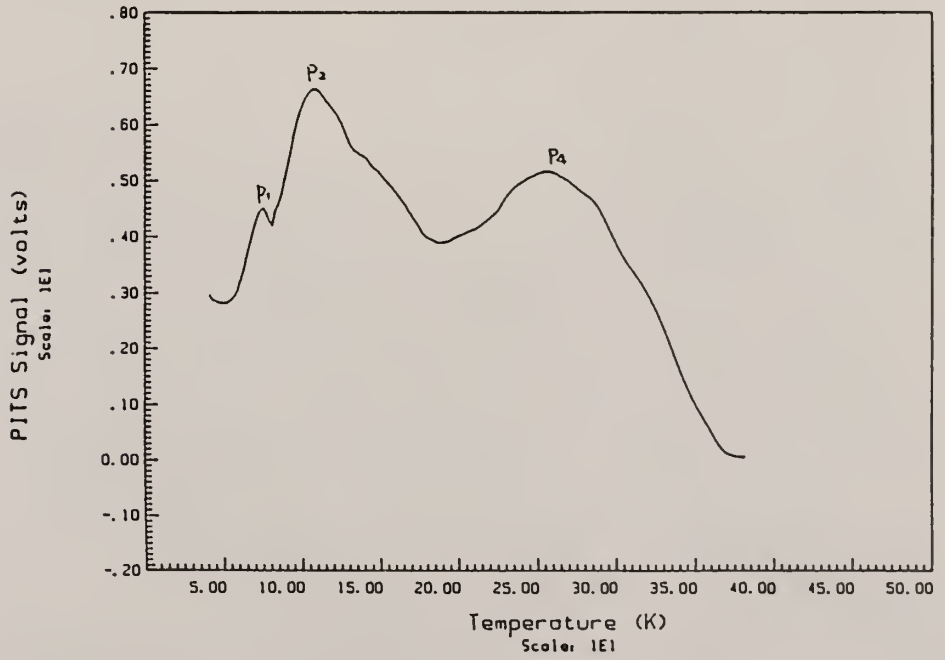

(b)

Fig. 3.4 PITS spectra of Se-GaAs (2.2×10^{12} cm^{-2}) at t_1 = 0.3 ms and t_2 = 2.4 ms
a) PLA sample (I=0.30 Jcm-2) b) FA sample

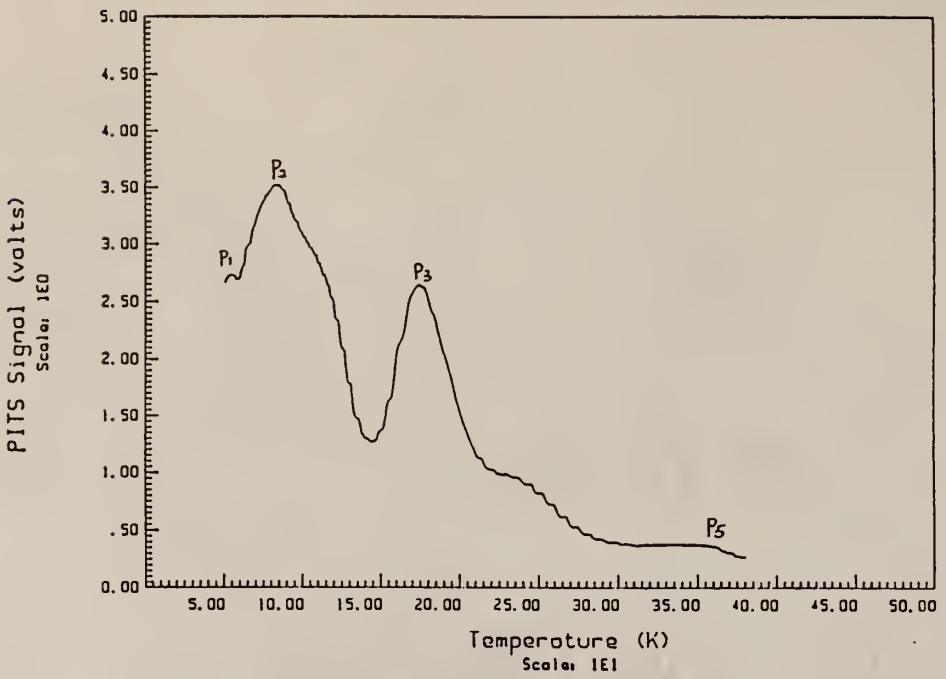

(a)

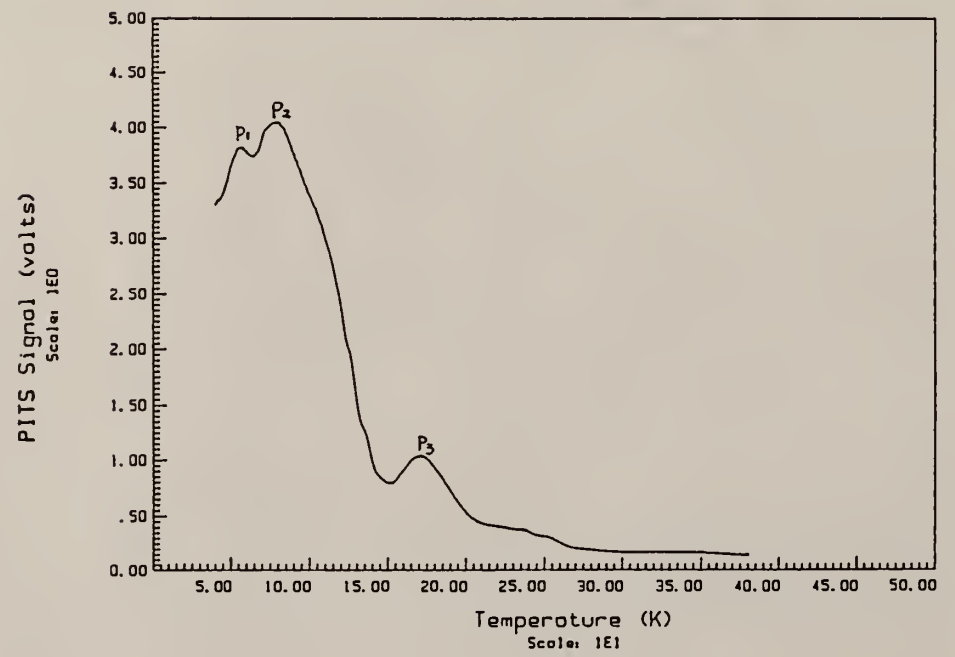

(b)

Fig. 3.5 PITS spectra of PLA (I=0.32 Jcm-2) Si-GaAs at t_1 = 0.3 ms and t_2 = 2.4 ms
a) dose=2.0 10^{13} cm^{-2} b) dose=1.0 10^{14} cm^{-2}

Table 3.2). The origins of these defects are unknown. The peak marked P_3 present in PLA samples at temperature of 170 - 180 K was also observed by Y. Yuba, and level 0.23 eV was obtained by R. E. Kremer, respectively, for a similar peak. The corresponding activation energy varied from 0.23 eV[19] to 0.34 eV[16] which resembles the property of an EL6 level. The values of E_t corresponding to peak P_3 for the samples varied between 0.23 and 0.34 eV (see Table 3.2). It is possible that the characteristics of crystal defects are affected by certain parameters of ion implantation and annealing processes.

The last two peaks P_2, and P_1 appear at very low temperature which correspond to deep level defects with a small activation energy (E_t < 0.1 eV). Similar defects have been observed before. For instance, level 0.15 eV at 108 K in F2212 was reported by R. D. Fairman [20] at 117 K in FA Se doped SI GaAs substrate. Some other levels such as 0.08 eV, 0.09 eV and 0.06 eV listed in Table 3.2 are close to some levels with small activation energy reported previously[17,21] in Shottky-barrier diodes fabricated on LPE (Liquid Phase Epitaxy) and bulk GaAs materials. The origin of these defects is unknown.

B. The Effectiveness of Dose Dependence and Emission Rate on the PITS Spectra of PLA Samples

As mentioned earlier, five peaks were observed in the PITS spectrum for high dose samples while the peak (P_5 at ~ 350 K) disappeared in low dose samples at t_1 = 0.3 ms and t_2 = 2.4 ms. Therefore, the dose dependence is observed in the PITS spectra. By making another PITS scan with a small emission rate (800 s^{-1}), the peak (P_5) that disappeared before shows up at 325 K (see Fig. 3.6) this time. But the peak (P_1) that is shown at 60 K in a PITS scan with a 3000 s^{-1} emission rate turns out to be a shoulder. Thus, the shape of the PITS spectrum is

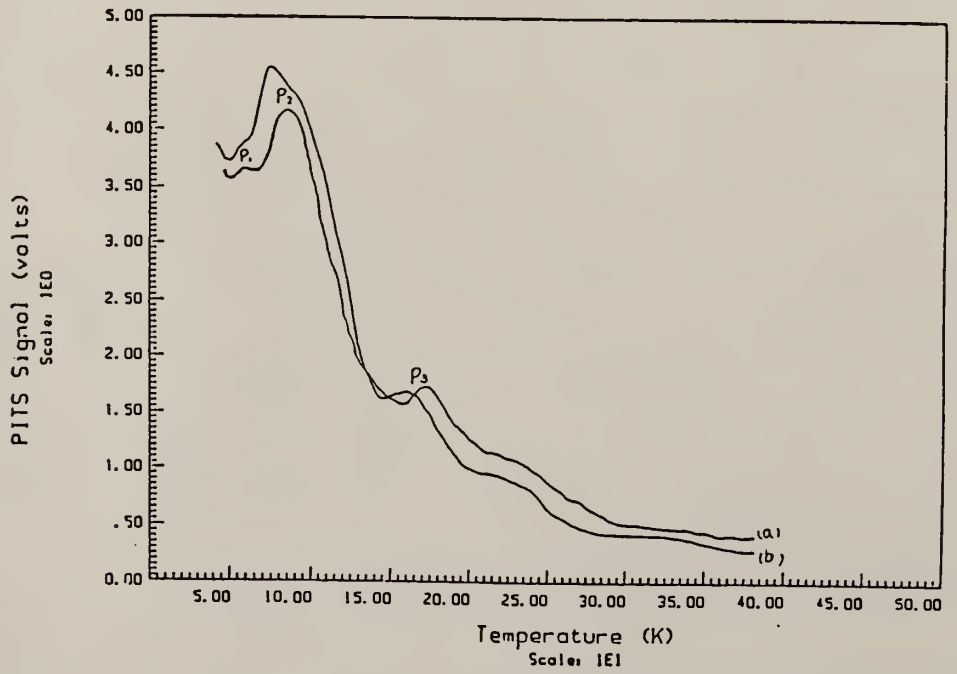

Fig. 3.6 PITS spectra of PLA (I=0.30 Jcm-2) Se-GaAs (2.2×10^{12} cm^{-2})
a) emission rate = 3000 1/s
b) emission rate = 800 1/s

dependent on the emission rate. The shallower level shows up with a big emission rate since it is close to the conduction band and the trapped carriers get emitted quickly. And oppositely, the deeper level is far away from the E_c and the trapped carriers get emitted slowly. This makes the deep level sensitive to a small emission rate. To ensure a proper characterization of all traps located in the semiconductor materials, the best way is to choose a proper emission rate for each PITS scan. Hopefully, this will lead to the accurate PITS measurement.

3.3 Comparison Between Pulsed Laser Annealing and Furnace Annealing on n-type GaAs

Three furnace annealed samples, F4012, F6014 and F2212, were compared with three PLA samples with the same implanted dose. Table 3.3 list all the results of the Hall effect and PITS experiments for these two sets of samples. The trap density has been described in relative units because it was not possible to obtain a quantitative answer. The penetration depth of laser light, the quantum efficiency of photons, and the actual area of samples were not precisely known. The fraction of traps totally filled with electrons by applied laser pulse was difficult to determine. The area of FA samples was approximately twice as large as of the PLA samples. The amplitude of the peak

Table 3.3 Characteristics in PLA and FA GaAs

	PLA			FA		
Sample	Se- GaAs	Si-GaAs		Se-GaAs	Si-GaAs	
dose(cm^{-2})	$2.2x10^{12}$	$4.0x10^{12}$	$6.0x10^{14}$	$2.2x10^{12}$	$4.0x10^{12}$	$6.0x10^{14}$
Sheet carrier density (cm^{-2})	$7.6x10^{13}$	$1.1x10^{14}$	$1.2x10^{14}$	$1.3x10^{12}$	$2.9x10^{12}$	$8.0x10^{13}$
Dose/N_s	59%	74%	13%	>100%	>100%	>100%
mobility (cm^2/s-V	270	250	290	2825	1970	1120
Active Layer (nm)	~60	--	--	~300	--	400
Trap Levels (eV) Hall & van der Pauw 0.02-0.07	small	small	small	vy. small	vy. small	vy. small
0.07-0.2	large	large	medium	medium	medium	medium
0.2 - 0.3	medium	medium	medium	none	none	none
0.3 - 0.6	trace	trace	trace	medium	medium	medium
0.7 - 0.8	small	small	medium	none	none	vy. small

-- no profiling experiment.

on PITS spectrum is proportional to the fraction of trap density N_{TT} which contributes to the emission process and is inversely proportional to sample area. The comparisons are conducted as follows:

1. Carrier activation and electron mobility

From the Hall data listed in Table 3.3, it can be noticed that the PLA samples have high sheet carrier concentration, which exceeds the implanted dose for the low dose PLA samples. The mobility of FA samples is $\sim 10^3$ $cm^2/V\text{-}s$ which is a few times larger than that of PLA samples.

2. The carrier distribution

Fig. 3.7 and Fig. 3.8 show the carrier and mobility distribution of sample F2212 and F6014. The profile of sample F2212 follows closely the theoretical LSS profile for the ion implantation process, and the profile of sample F6014 indicates that a significant out-diffusion has occurred. The active layer has a thickness of 300 nm - 400 nm which is several times deeper than for the PLA sample. The mobility of the FA sample is quite high.

3. The correlations between defects and electrical properties.

The activation energy of deep levels and their origins in both PLA and FA samples were discussed in section 3.2A. In this section the trap density and the correlation between defects and electrical properties are

discussed.

It can be seen in Table 3.3 that the trap density of PLA samples are slightly higher than that of FA samples except for the level o.56 eV, in which there was only a trace peak in PLA samples. There is zero trap density for the level at 0.8 eV for low dose FA samples. This level is related to heavy implanted damage (see section 3.2). The low dose furnace annealed samples did not have this damage, which lead to a high electron mobility (see Table 3.3). The high dose furnace annealed sample had a very small amount of this damage, which resulted in lower activation and lower mobility. Since high dose PLA sample had a medium density of this defect, it had low mobility and low activation. Over all comparison of furnace and pulsed laser annealed samples showed that the defect density in the PLA samples was higher, which gave lower electron mobility.

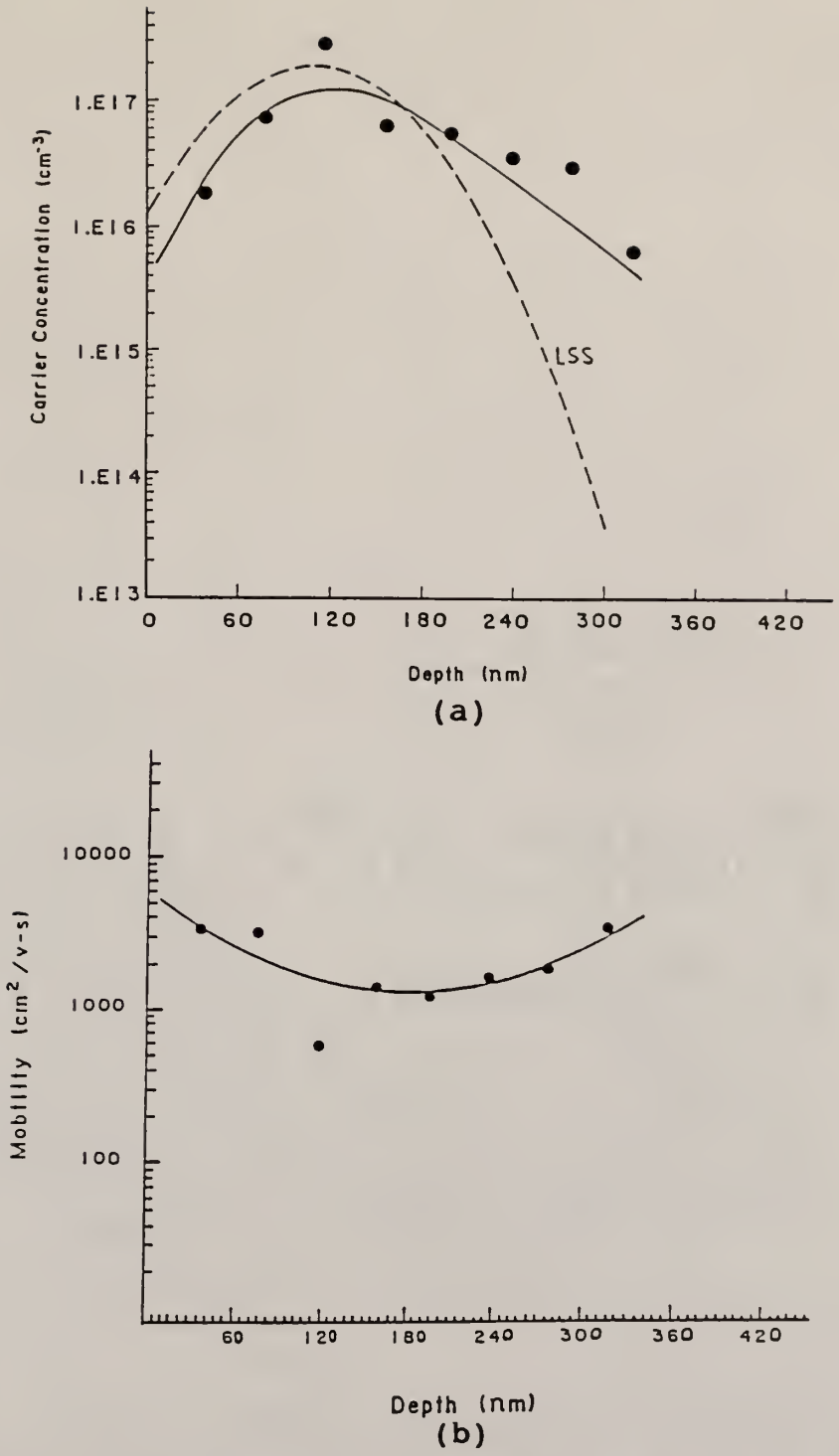

Fig. 3.7 Depth profiling of FA Se-GAAs (2.2 x 10^{12} cm^{-2}) a) Carrier concentration b) Electron mobility The solid lines were drawn through the data points as a visual aid only.

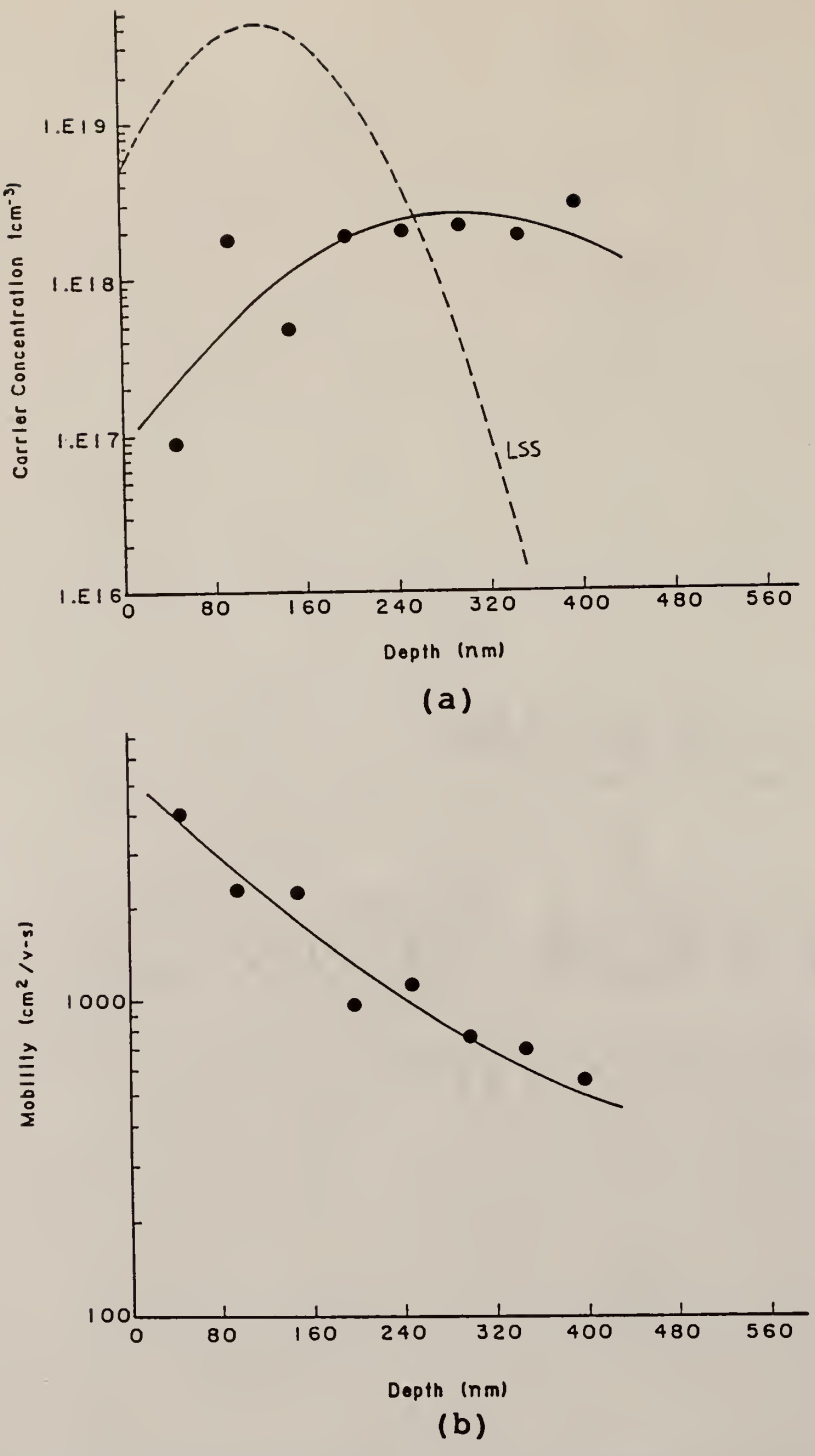

Fig. 3.8 Depth profiling of FA Si-GAAs (6.0 x 10^{14} cm^{-2}) a) Carrier concentration b) Electron mobility The solid lines were drawn through the data points as a visual aid only.

IV. SUMMARY AND CONCLUSION

A study of carrier activation and deep level defects was performed in n-type GaAs implanted with Se (at 320 keV) to a dose of 2.2×10^{12} and with doses of Si (at 140 keV) from 4×10^{12} to 6×10^{14} cm^{-2} through a silicon nitride cap. The samples were annealed using a pulsed XeCl excimer laser (λ = 308 nm) with a pulse duration of 12 ns and light intensity from 0.23 to 0.32 Jcm^{-2}. The electron concentration and mobility were studied by means of Hall effect and van der Pauw measurements. Despite a success in carrier activation, the over-all electron mobility increased with higher laser light intensity. The surface morphology of pulsed-laser-annealed samples affected their electrical properties and the mobility, in particular. The PLA process introduced additional impurities from the passivation layer.

Four different doses (4×10^{12} - 6×10^{14} cm^{-2}) of Si implanted GaAs were analyzed after PLA process at 0.32 Jcm^{-2} laser energy by the photo-induced transient spectroscopy (PITS) measurements as well as by Hall and van der Pauw techniques to determine the correlations between electrical properties and defect levels. Some furnace annealed samples were characterized as a reference. A high carrier activation was achieved in both

low dose and high dose PLA samples; however, the high carrier density, high trap density and heavy implant damage resulted in a low electron mobility of the samples. Contrarily, a fairly high activation and high electron mobility were reported in low dose FA samples. These FA samples had smaller defect density. In high dose samples, the furnace annealing process was not very effective.

Three deep levels, 0.30 eV, 0.56 eV and 0.80 eV, were characterized in both pulsed laser and furnace annealed samples. In addition, two shallower defect levels were detected in each of the tested samples. Even though PITS is a relatively new technique for characterization of defect levels and is less sensitive to deep levels compared with capacitance DLTS[16], it is still a very useful technique for characterization of deep levels on semiconductor substrates where the fabrication of rectifying junction is difficult.

This study shows that pulsed laser annealing can produce doping from a capping layer by the laser melting process without the need for an ion-implantation step. However, it appears that significant numbers of defects are introduced by a silicon nitride layer. Other capping layers might yield better results. In general, the residual implanted damage which remains either in capped PLA samples or capless PLA samples[5] causes low mobility of

n-type GaAs. But the capped pulsed laser annealing process which results in a very high doping density, as determined by Raman spectroscopy on small (spot laser annealed) samples by A. Rys and A. Compaan et. al.[26], could prove to be a very useful technique for nonalloyed ohmic contacts.

REFERENCES

1. David K. Ferry, Editor-in-Chief, "Gallium Arsenide Technology", SAMS.

2. S.M.Sze, "SEMICONDUCTOR DEVICES Physics and Technology" Wiley Interscince.

3. Ghandhi, "VLSI Fabrication Principles, Si and GaAs" Wiley Interscince.

4. Shunji Nojima, "Laser annealing effects in ion-implantation GaAs", J. Appl. Phys. 53(7),July, 1982.

5. Ahmed H. Oraby,* Yoshihiko Yuba, Mikio Takai,Kenji Gamo and Susumu Namba, "Pulsed Laser Annealing Effects in Si-Implanted GaAs", J. Appl. Phys. 1983 pp.326.

6. N.J. Barrett and J.D. Grang, "Annealing of selenium-implanted GaAs", J. Appl. Phys. 56(12), Dec. 1984.

7. R. T. Young, J. Narayan, W.H. Christie, G.A. van der Leeden, J.I. Levatter, L.J. CHeng, "Semiconductor Processing with Excimer Laser", Solid State Technology/ Nov. 1983.

8. Sukhdev S. Gill and B.J. Sealy, "Review of Rapid Thermal Annealing of Ion Implanted GaAs", J. Electrochem. Soc. Dec. 1986.

9. Timothy W. H. CHIN, "A Study of Hall-Effect Measurement Techniques on Pulsed Laser Annealed Gallium Arsenide", A Master's Thesis Kansan State University 1988.

10. Van der Pauw, "A METHOD OF MEASURING THE RESISTIVITY AND HALL COEFFICIENT ON LAMELLAE OF ARBITRARY SHAPE", PHILIPS TECHNICAL REVIEW, VOL. 20, Feb. 1958.

11. J.W. Mayer et al, "ION IMPLANTATION OF SILICON" Canadian Journal of Physics. Volume 45 (1967).

12. Shinya Lida and Kazuhiro Ito, "Selective Etching of Gallium Arsenide Crystals in H_2SO_4-H_2O_2-H_2O System", J. Electrochem. Soc. May 1971.

13. D.V. Lang, "Deep-level transient spectroscopy: A new method to characterize traps in semiconductors", J. Appl. Phys., Vopl.45,No. 7, July 1974.

14. Sunanda Dhar et al, "Nature and distribution of electrically active defects in Si-implanted and lamp-annealed GaAs", J. Appl. Phys. 58(11), 1 Dec. 1985.

15. Ch. Hurtes et al, "Deep-level spectroscopy in high-resistive materials", Appl. Phys. Lett. 32(12), 15 June 1978.

16. Y. Yuba et al, "Deep levels in implanted and laser annealed GaAs studied by current and capacitance-transient measurements", Inst. Phys. Conf. Ser. No. 63: Chapter 5 1981.

17. S. J. Pearton et al, "Deep traping Centers in n-GaAs Surface Barrier Diodes for Nuclear Radiation Detection", Electronics Letters 5th June 1980 Vol.16 No. 12.

18. G. M. Martin et al, "Electron Traps in Bulk and Epitaxial GaAs Crystals" Electronics Letters 13, 666-668 (1977).

19. R. E. Kremer et al, "Transient photoconductivity measurements in semi-insulating GaAs.", J. Appl. Phys. 62 (6), 15 Sep. 1987.

20. Robert D. Fairman et al, "Growth of High-Purity Semi-Insulating Bulk GaAs for Integrated-Circuit Applications", IEEE Transactions on electron devices, vol. ED-28, No. 2, Feb. 1981.

21. G. N. Maracas,"DLTS analysis of GaAs MESFETS and effects of deep levels on devices proformance", A doctoral dissertation Cornell University 1982.

22. C. T. Sah et al, "Thermal and optical emmision and capture rates and cross sections of electrons and holes at imperrfection centers in semiconductors from photo and dark junction current and capacitance experiments", Solid-State Electronics Pergamon Press 1970. Vol. 13, pp. 759-788.

23. Installation, operation and servicing instructions, CRYO-TORR (R) 7 HIGH-VACUUM PUMP, (UTILIZING A MODEL 22 COLD HEAD) MAY 1984.

24. Model 162 boxcar averager, operating and service manual, EG&G princeton applied research.

25. Technical Data DT-470 Series Temperature Sensors, Lake Shore Coyoteonics Inc.

26. A. Rys et al, "Very heavily doped n-type GaAs obtained with pulsed laser annealing", Proceedings of SPIE-T International Society for Optical Engineering: Advanced Processing of Semiconductor Devices II, Vol. 945, pp. 41.

27. T Itoh and H Yanai, "Experimental Investigation of Interface Traps in GaAs Planar Devices by DLTS and PITS Methods." Inst. Phys. Conf. Ser. No.56: Chapter 8

APPENDIX A

Remarks on the Measurements

The experiment for this course of study mainly deals with GaAs sample measurements. Therefore, the comments will focus on GaAs samples and the measurements.

GaAs SAMPLES

* The nitride cap lost its original thickness after undergoing pulsed laser annealing process. The etching time of silicon nitride cap coated on the sample should be shortened.
* The surface of laser annealed sample should be shiny and a full clover leaf pattern should be visible on the sample.
* Due to sensitive surface of annealed sample, using silicone adhesive to protect the indium contacts from the etchant affects the results of Hall measurements.

MEASUREMENTS

* Due to a permanent magnetic field remaining in the half-inch gap of the electro-magnet, the static Hall voltage readings must be taken outside of the gap.
* To etch off the Si-GaAs, the proper volume ratio of the etchant (see section 2.3)should be chosen.

* Due to a 156°C melting temperature of indium, the temperature of PITS cannot go further than 400 K which is 127°C.
* There were two noise sources in PITS measurements, one was from bad contacts formed and the other was due to the system vibrations. To prevent these noise, the indium contacts should be well sintered and the copper must be soldered properly with the indium contacts.

APPENDIX B

Calculation for Activation Energy and Capture cross Section

As described in section 2.5, the E_t and σ_n can be obtained by knowing the slope and intercept of the Eq. 2.5.18. To draw a line based on the Eq. 2.5.18 from the PITS measurements, four PITS-scan with different sampling gate settings were run for each tested sample. The emission coefficient and maximum peak temperature were recorded for each PITS-scan and each sample, respectively. A set of peak temperatures and the corresponding emission coefficients for every tested sample are listed in the next few pages. A program called "LINFIT" was applied to perform a linear fit according to a set of emission coefficients and peak temperatures since the data points from the experiment were not accurate enough to form a linear line. Finally, the slope and intercept of the linear line were obtained from the "LINFIT". The E_t and σ_n are expressed as follows:

$$E_t = \text{slope} * 1000 * k$$

$$\sigma_n = \exp(\text{interception})/\gamma_n$$

where $k = 8.86 \times 10^{-5}$ eV and $\sigma_n = 1.9 \times 10^{-20}$ $cm^{-2}k^{-2}s^{-1}$.

Sample number: L4012
Sample type : Pulsed laser annealed Si-GaAs
Ion implantation dose: 4.0 e12 cm-2
Laser intensity: 0.32 Jcm-2

τ(ms)	T_m(K)	$1000/T_m(K^{-1})$	$T_m^2\tau(K^2s^{-1})$	$\ln(T_m^2\tau)$
0.7	64	15.55	2.89	1.06
0.5	64	15.43	2.10	0.74
0.3	64	15.50	1.25	0.22
0.15	66	15.10	0.65	0.42
0.7	83	11.93	4.92	1.59
0.5	84	11.81	3.59	1.28
0.3	86	11.59	2.23	0.80
0.15	94	10.73	1.30	0.26
0.7	173	5.77	20.99	3.04
0.5	172	5.78	14.94	2.70
0.3	180	5.57	9.66	2.27

Sample number: L2013
Sample type : Pulsed laser annealed Si-GaAs
Ion implantation dose: 2.0 e13 cm-2
Laser intensity: 0.32 Jcm-2

τ(ms)	T_m(K)	1000/T_m(K^{-1})	$T_m^2\tau$(K^2s^{-1})	ln($T_m^2\tau$)
0.6	55	18.02	1.84	0.61
0.5	57	17.30	1.67	0.51
0.3	60	16.69	1.07	0.54
0.15	60	15.58	0.54	-0.60
0.6	78	12.80	3.66	1.29
0.5	81	12.30	3.28	1.19
0.3	83	12.03	2.07	0.38
0.15	86	11.66	1.10	0.10
0.6	173	5.77	21.05	3.05
0.5	176	5.67	15.45	2.74
0.3	180	5.56	9.70	2.27

Sample number: L1014
Sample type : Pulsed laser annealed Si-GaAs
Ion implantation dose: 1.0 e14 cm-2
Laser intensity: 0.32 Jcm-2

τ(ms)	T_m(K)	$1000/T_m(K^{-1})$	$T_m^2\tau(K^2s^{-1})$	$\ln(T_m^2\tau)$
0.7	55	18.00	2.15	0.77
0.5	57	17.42	1.65	0.49
0.3	58	17.09	1.03	0.03
0.5	79	12.59	3.15	1.15
0.3	83	12.05	2.07	0.73
0.15	87	11.47	1.14	0.13
0.5	170	5.89	14.38	2.66
0.3	175	5.71	9.18	2.22
0.15	180	5.54	4.87	1.54
0.5	340	2.94	57.80	4.05
0.3	346	2.89	35.95	3.58
0.15	355	2.82	18.90	2.94

Sample number: L6014
Sample type : Pulsed laser annealed Si-GaAs
Ion implantation dose: 6.0 e14 cm-2
Laser intensity: 0.32 Jcm-2

τ(ms)	T_m(K)	$1000/T_m(K^{-1})$	$T_m^2\tau(K^2s^{-1})$	$\ln(T_m^2\tau)$
0.7	46	21.74	1.48	0.39
0.5	48	20.70	1.17	0.15
0.15	50	19.88	-0.38	-0.97
0.7	82	12.25	4.66	1.54
0.5	84	11.89	3.54	1.26
0.3	86	11.61	2.22	0.79
0.7	169	5.91	20.01	2.99
0.5	172	5.82	14.74	2.69
0.3	174	5.72	9.15	2.21
0.15	185	5.41	5.12	1.63

Sample number: L2212
Sample type : Pulsed laser annealed Se-GaAs
Ion implantation dose: 2.2 e12 cm-2
Laser intensity: 0.304

τ(ms)	T_m(K)	1000/T_m(K^{-1})	$T_m^2\tau$(K^2s^{-1})	ln($T_m^2\tau$)
1.25	53	18.62	3.60	1.28
1.0	56	17.82	3.14	1.14
0.7	58	17.24	2.35	0.85
0.3	62	16.13	1.15	0.14
1.25	73	13.70	6.66	1.89
1.0	78	12.82	6.08	1.81
0.7	80	12.50	4.48	1.49
0.3	86	11.53	2.25	0.81
1.25	162	6.15	33.09	3.49
1.0	165	6.06	27.22	3.30
0.7	166	6.01	19.40	2.96
0.3	173	5.78	8.96	2.19

Sample number: F4012
Sample type : Furnace annealed Si-GaAs
Ion implantation dose: 4.0 e12 cm-2
Laser intensity: none

τ(ms)	T_m(K)	1000/T_m(K^{-1})	$T_m^2\tau$(K^2s^{-1})	ln($T_m^2\tau$)
0.5	53	18.62	1.44	0.36
0.3	57	17.45	0.98	-0.01
0.15	66	15.08	0.65	-0.41
0.5	102	9.18	5.19	1.64
0.3	107	9.33	3.45	1.24
0.15	119	8.39	2.13	0.76
0.5	265	3.76	35.25	3.56
0.3	273	3.66	22.41	3.11
0.15	277	3.60	11.56	2.45
0.5	273	3.66	37.24	3.62
0.3	279	3.57	23.42	3.15
0.15	285	3.50	12.22	2.50

Sample number: F6014
Sample type : Furnace annealed Si-GaAs
Ion implantation dose: 6.0 e14 cm-2
Laser intensity: none

τ(ms)	T_m(K)	1000/T_m(K^{-1})	T_m^2/τ(K^2s^{-1})	ln(T_m^2/τ)
0.7	88	11.33	5.46	1.70
0.5	91	10.95	4.17	1.43
0.3	94	10.62	2.67	0.98
0.15	97	10.26	1.43	0.35
0.7	252	3.96	44.59	3.79
0.5	260	3.83	34.03	3.53
0.3	268	3.72	21.69	3.08
0.15	280	3.58	11.73	2.46
0.7	355	2.81	88.46	4.48
0.5	349	2.86	60.97	4.11
0.3	343	2.91	35.38	3.57

Sample number: F2212
Sample type : Furnace annealed Se-GaAs
Ion implantation dose: 2.2 e12 cm-2
Laser intensity: none

τ(ms)	T_m(K)	$1000/T_m(K^{-1})$	$T_m^2\tau(K^2s^{-1})$	$\ln(T_m^2\tau)$
0.7	66	15.15	3.05	1.11
0.5	67	14.81	2.28	0.82
0.3	70	14.16	1.49	0.40
0.15	74	13.40	0.83	-0.18
0.7	103	9.67	7.48	2.01
0.5	105	9.48	5.57	1.72
0.3	108	9.25	3.51	1.25
0.15	112	8.86	1.91	0.64
0.7	233	4.28	38.26	3.64
0.5	237	4.21	28.20	3.34
0.3	246	4.06	18.21	2.90
0.15	254	3.92	9.74	2.28

APPENDIX C

Error Estimation of Activation Energy and Capture Cross Section in PITS Measurements

The error sources considered in PITS measurements for E_t and σ_n error estimation are based on Eq. 2.5.17 i.e.

$$T_m^2 = (\gamma_n \sigma_n)^{-1} + E_t/kT_m$$

Obviously, the inaccurate E_t and σ_n values are either from erroneous temperature readings or t_1 readings. It has been found that temperature sensor is one of the error sources. In addition, the broad peak error also need to be included in inaccuracy of T_m. The broader the peak, the bigger the error will be. The error related to t_1 is from the boxcar. Then the specifications for above error sources are listed as follows:

1. temperature sensor[25]

   +-1K at 2 K - 100 K

   +-1% K at 100 - 400 K

2. peak temperature readings

   +-1 K T < 120 K

   +-2 K 120 K < T < 200 K

   +-3 K 200 K <= T < 300 K

   +-4 K 300 K <= T < 380 K

3. aperture delay range[24]

   +-2%

Making a sample calculation of P_1 on sample L1014,

τ' = +-2%,

T' = T +-1 +-1 = T +-2, T < 100 K

MAX.

τ(ms)	T'_m(K)	$1000/T'_m(K^{-1})$	$T_m'^2\tau'(K^2s^{-1})$	$\ln(T_m'^2\tau')$
0.714	57	17.39	2.36	0.86
0.510	59	16.83	1.79	0.59
0.306	60	16.53	1.12	0.11

MIN.

τ(ms)	T'_m(K)	$1000/T'_m(K^{-1})$	$T_m'^2\tau'(K^2s^{-1})$	$\ln(T_m'^2\tau')$
0.686	53	18.69	1.96	0.67
0.490	55	18.05	1.50	0.41
0.294	56	17.70	0.94	-0.06

Run "LINFIT" to find E_t(max), σ_n(max) and E_t(min), σ_n(min), then

E_t = 0.07 +/- 0.0058 eV

σ_n = 2.68 +/- 1.11x10^{-15} cm ^{2}

APPENDIX D

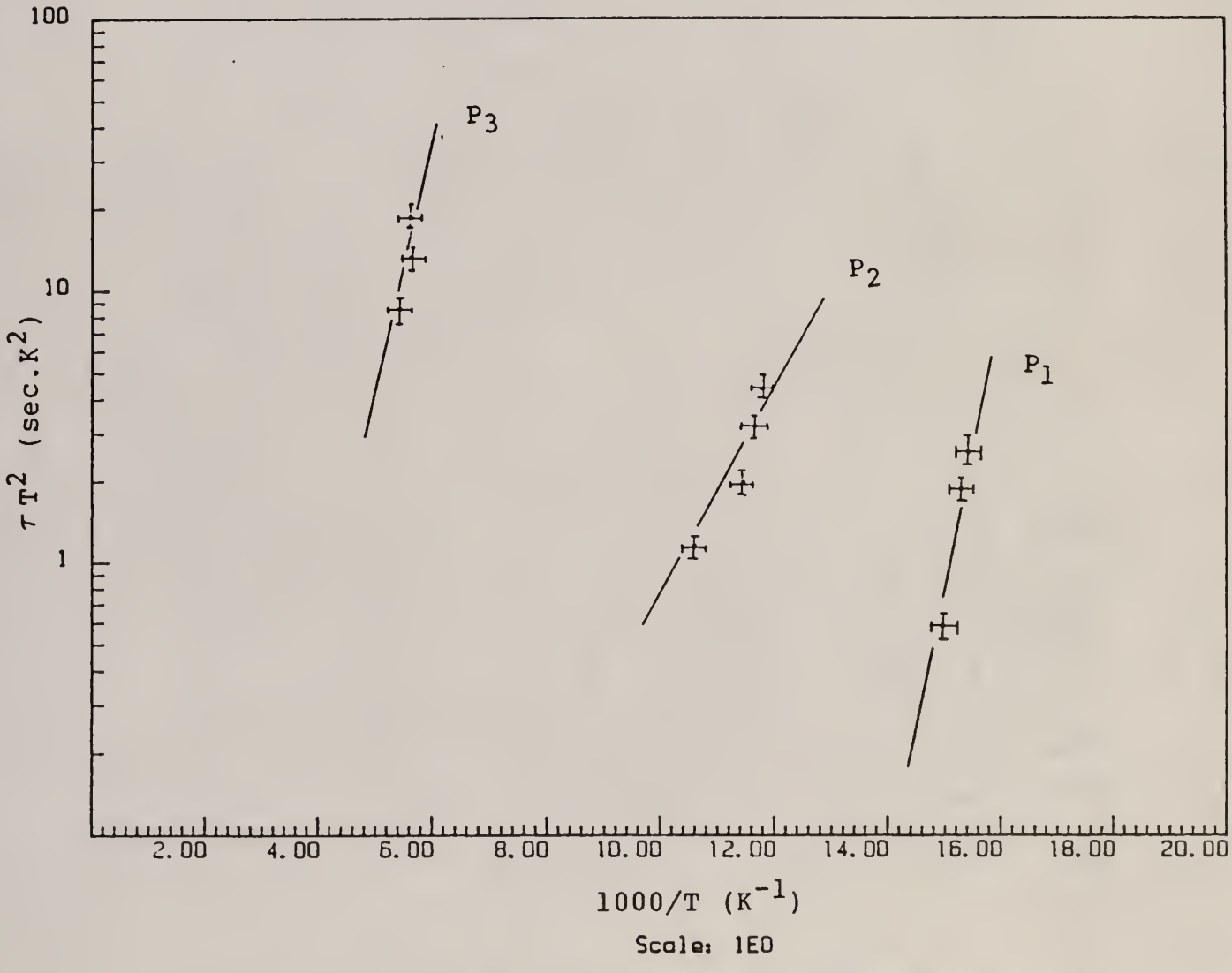

Fig. D.1 The Arrhenius plot of PLA (0.32 J/cm^2) Si-GaAs (4.0 el2 cm-2)

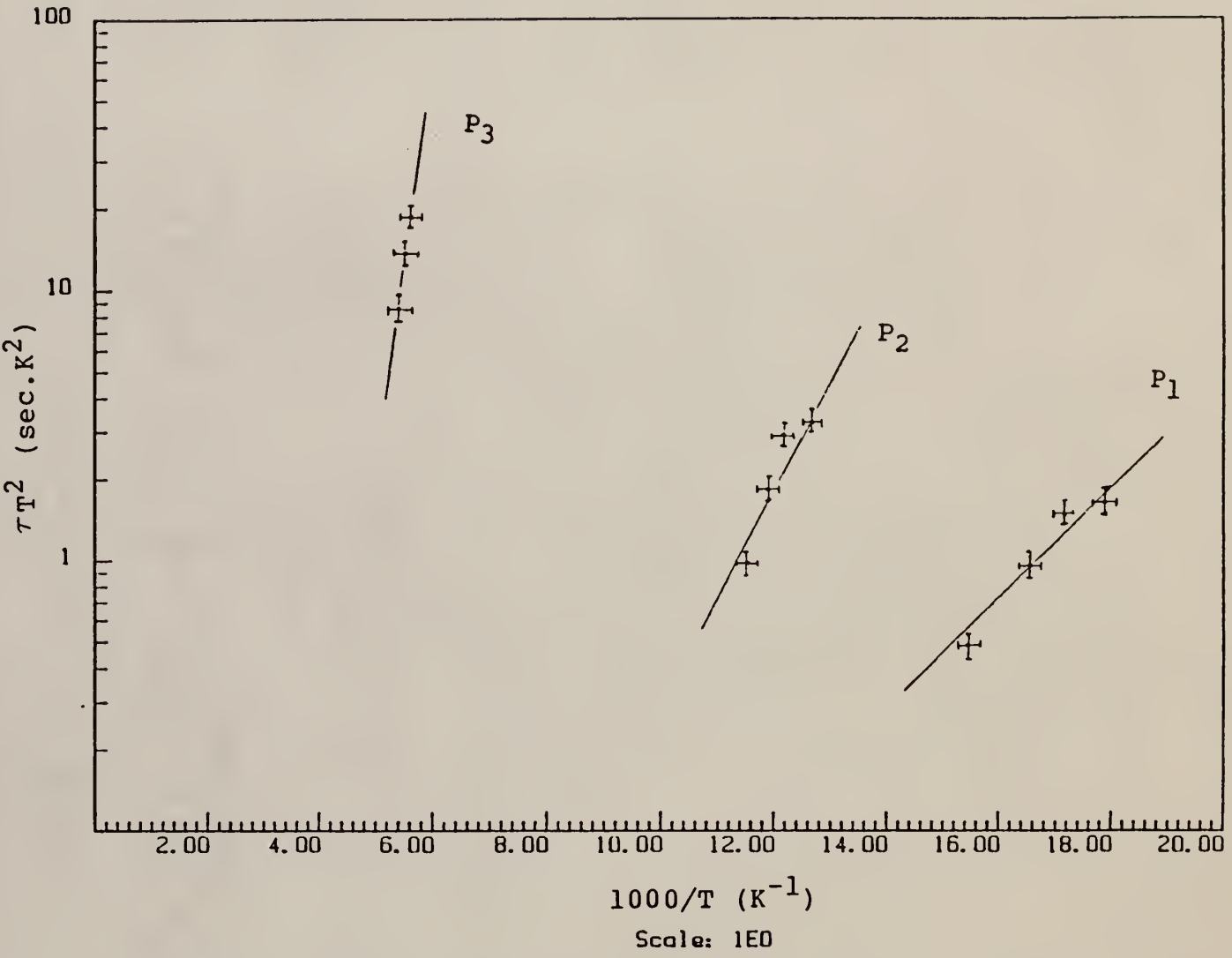

Fig. D.2 The Arrhenius plot of PLA (0.32 J/cm^2) Si-GaAs (2.0 e13 cm-2)

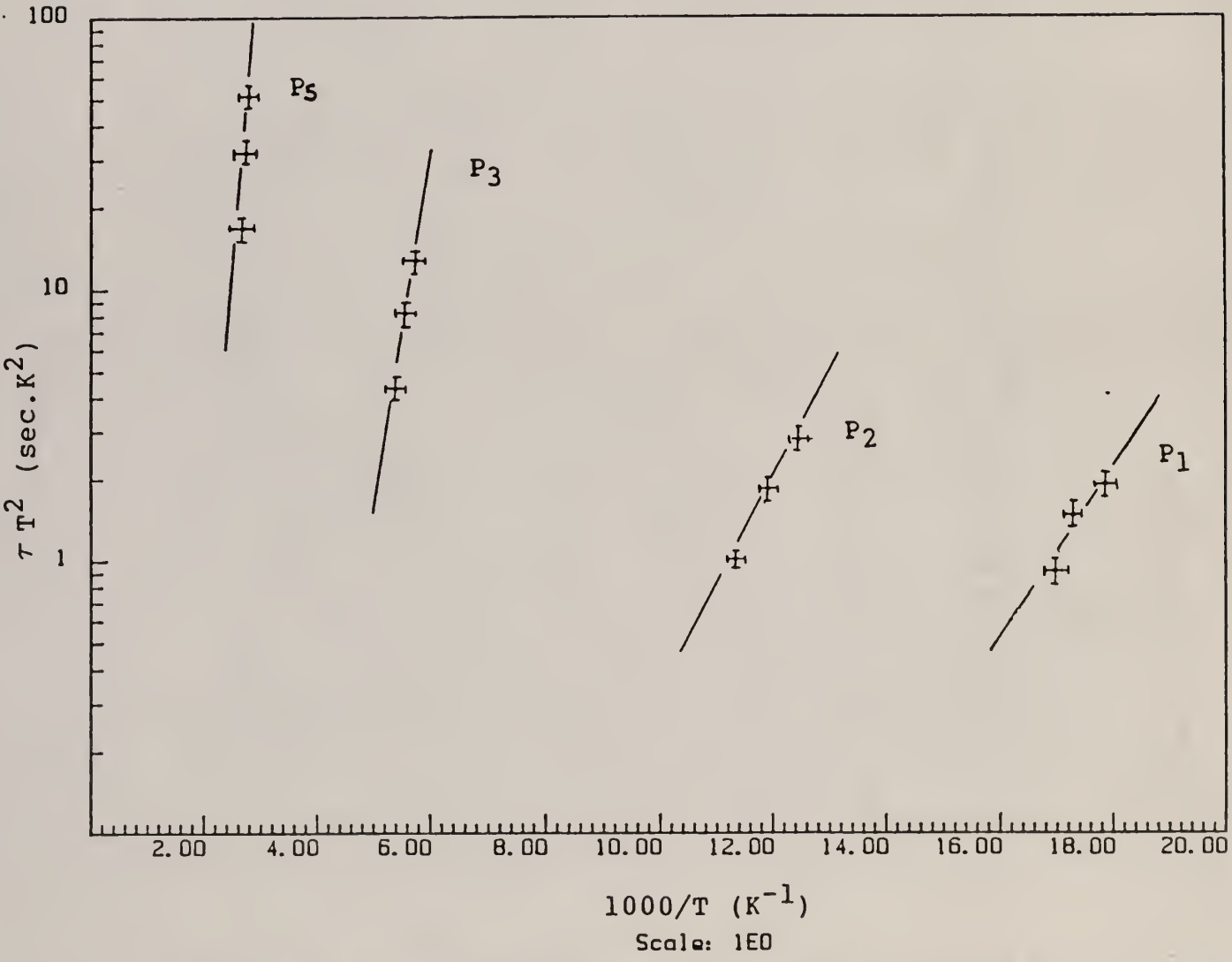

Fig. D.3 The Arrhenius plot of PLA (0.32 J/cm^2) Si-GaAs (1.0 e14 cm-2)

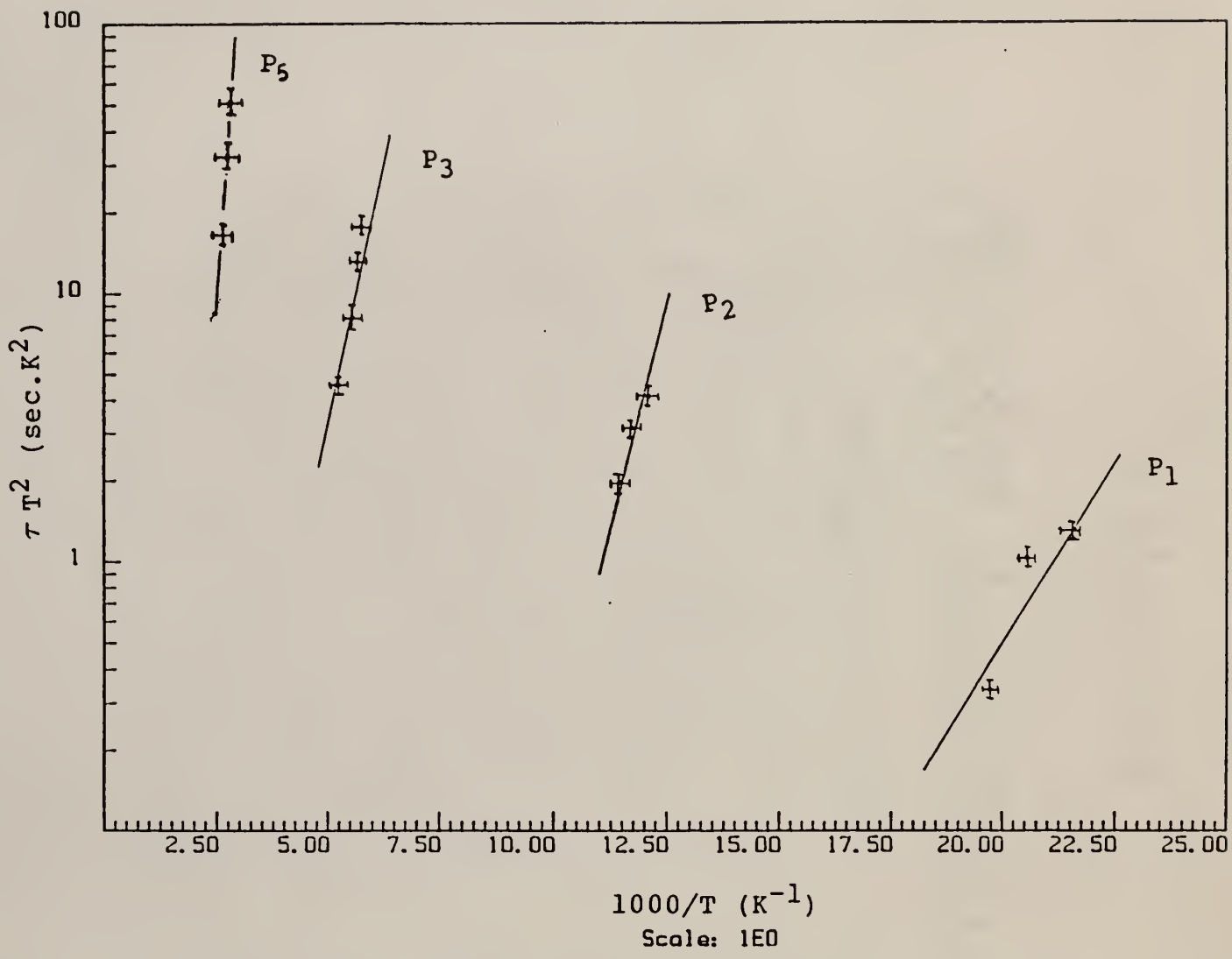

Fig. D.4 The Arrhenius plot of PLA (0.32 J/cm^2) Si-GaAs (6.0 el4 cm-2)

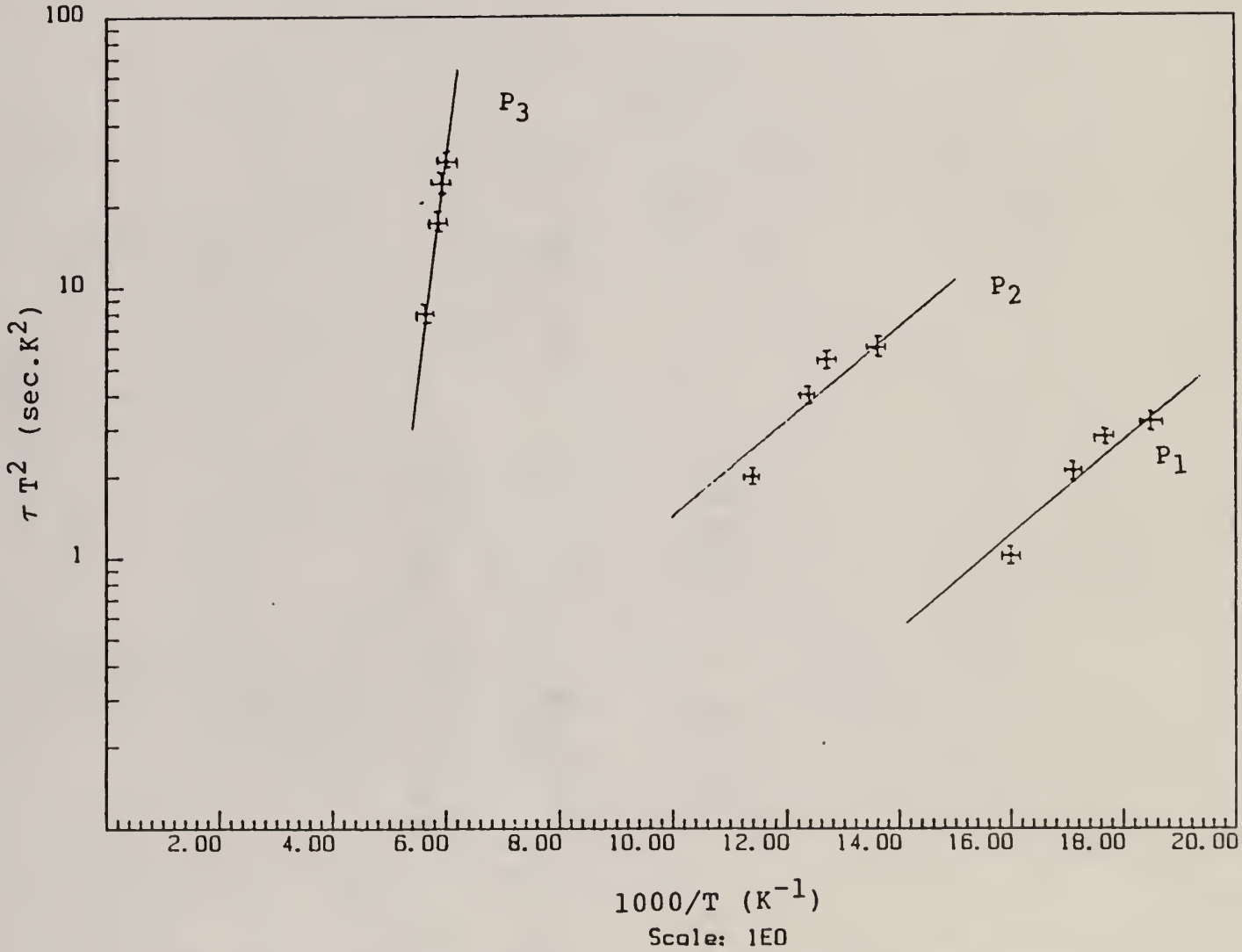

Fig. D.5 The Arrhenius plot of PLA (0.30 J/cm^2) Se-GaAs (2.2 el2 cm-2)

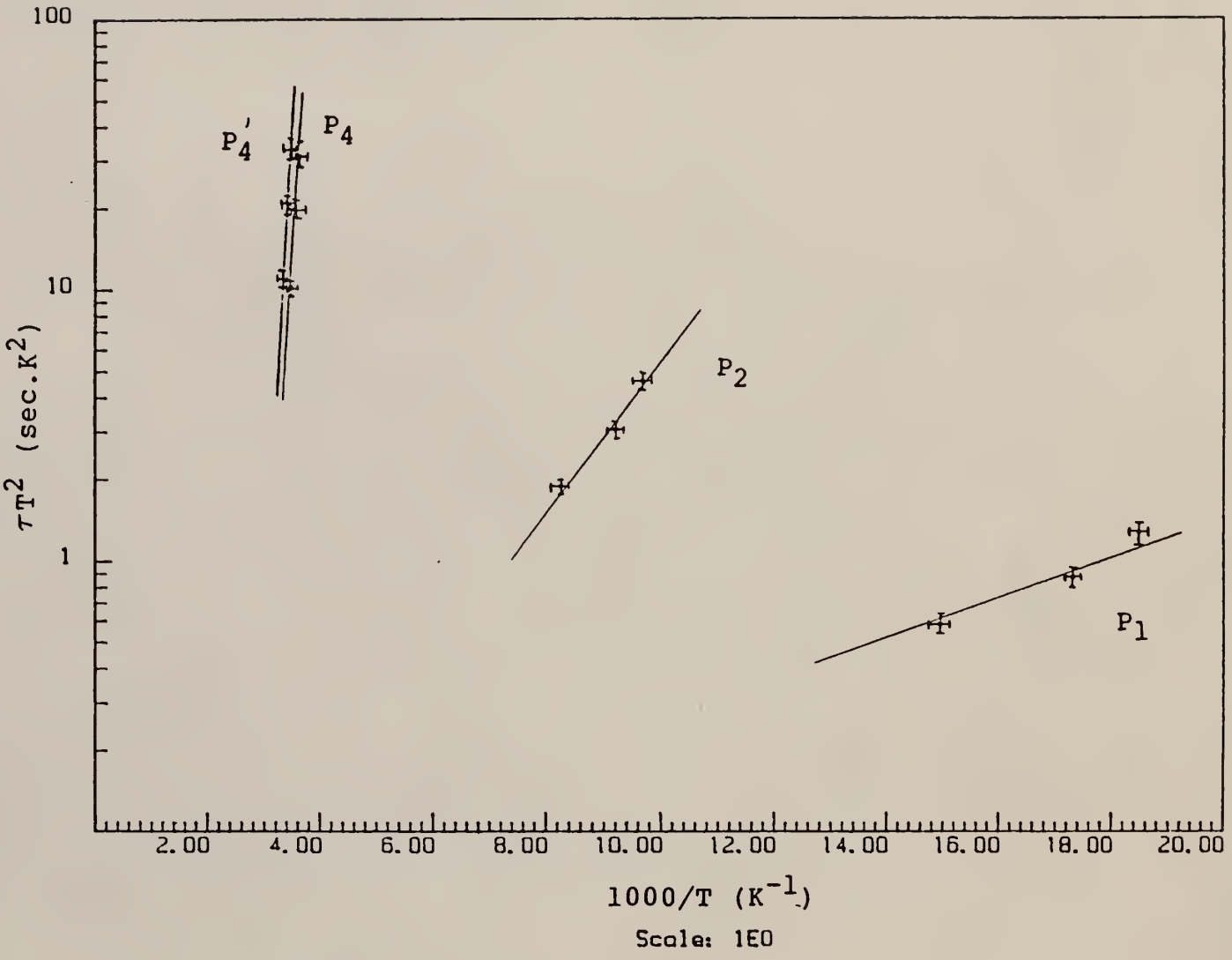

Fig. D.6 The Arrhenius plot of FA Si-GaAs (4.0 el2 cm-2)

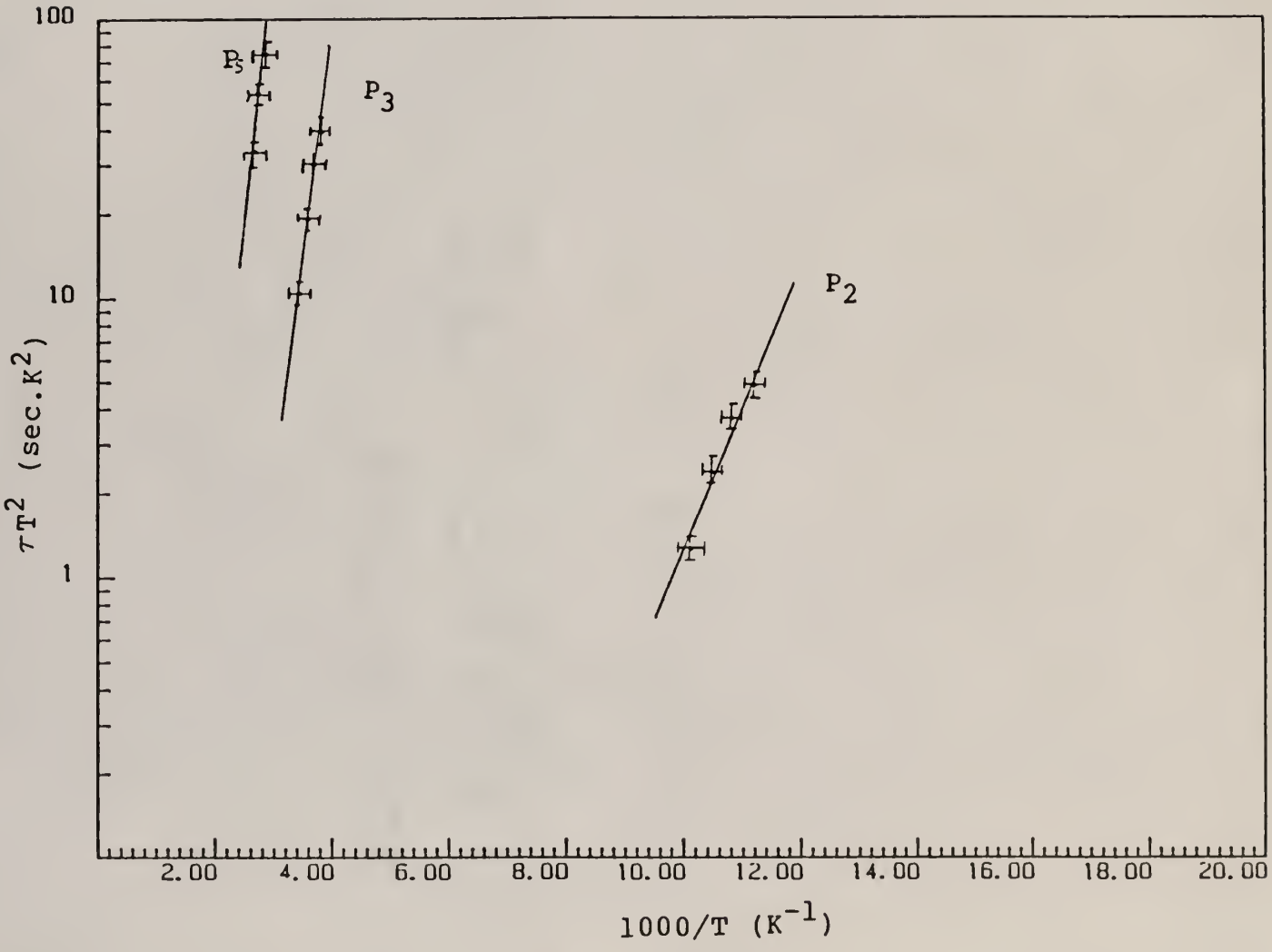

Fig. D.7 The Arrhenius plot of FA Si-GaAs (6.0 e14 cm-2)

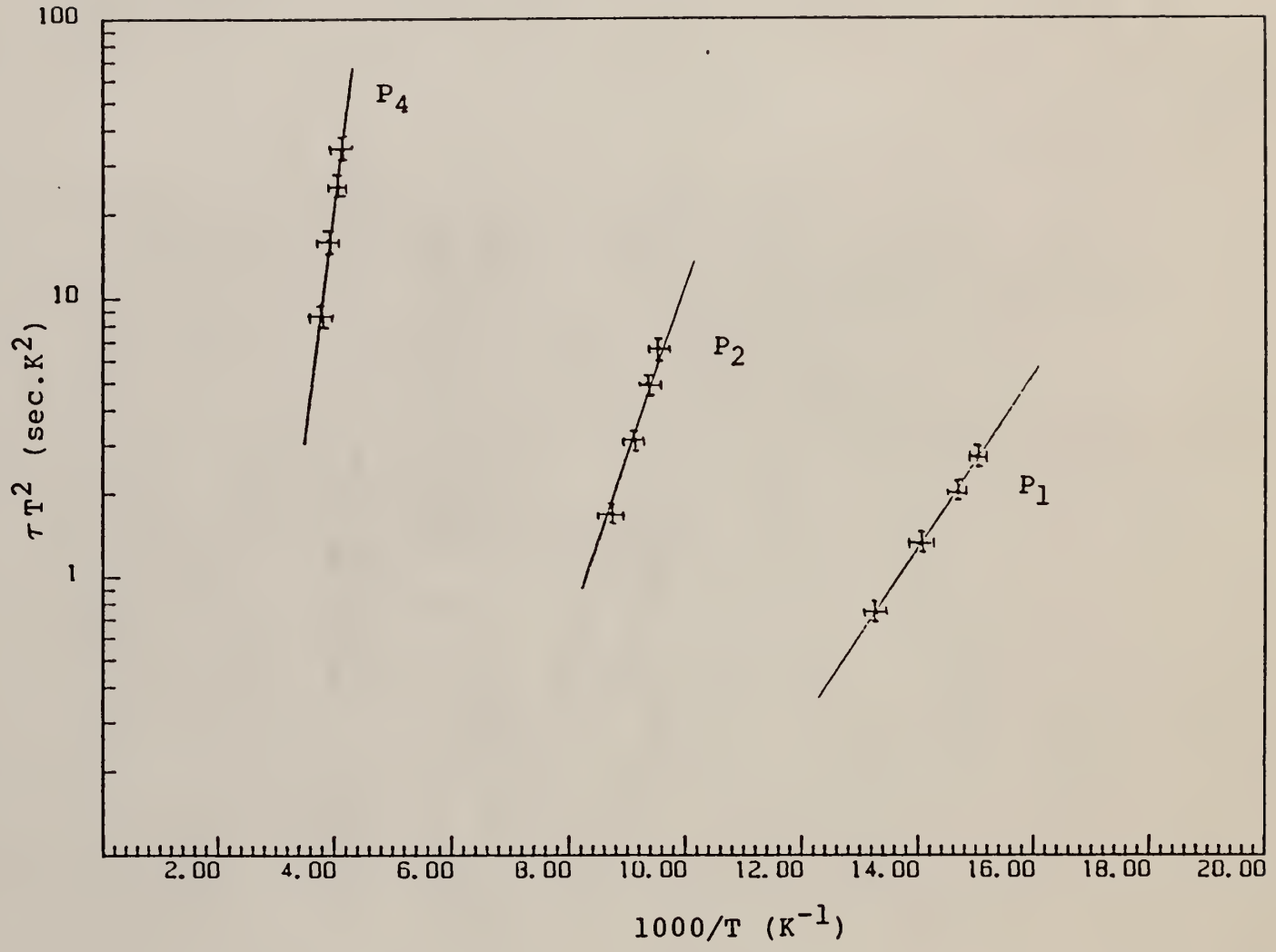

Fig. D.8 The Arrhenius plot of FA Se-GaAs (2.2 el2 cm-2)

APPENDIX E

```
10  ! ************************************************************************
15  !
20  ! Program Title: AUTO
30  !
40  ! Programmer: Yanan Shieh
50  !
60  ! Date: 03-23-1988
70  !
80  ! Version  1.0
90  !
100 ! Description: This program controls Fluke 8520A Digital Multimeter to
110 !              record voltage from GaAs sample automatically,calculates
120 !              those record data using some equations of solid state
130 !              field based on Van Der Pauw,Hall effect and etching
140 !              techniques: and plots the Depth  Profile.
150 !
160 ! Main Variable Description:
170 !
180 !       CURRENT()         Array of input current from current source.
190 !       F                 Correction factor for Van Der Pauw measurements.
200 !       No().Uo()         Array of electron mobility for n-type GaAs.
210 !       Ns()              Array of sheet carriers concentration.
220 !       Ps()              Array of sheet resistivity.
230 !       Ro(). Rb()        Resistance arrays for Hall Effect measurement.
240 !       Rhs()             Array of sheet Hall coefficient.
250 !       VOLT()            Array of voltage read out from sample by DVM each
260 !                         trigger time.
270 !       VOL()             Array of average voltage for one direction current.
280 !
290 ! ************************************************************************
300 DISP "PLEASE ANSWER ALL QUESTIONS BY PRESSING Y OR N!"
310 OPTION BASE 0
320 PRINTER IS 701
330 !
340 ! Declarations
350 !
360 REAL R(10),VOL(2),Rmnop(10),CHR(10),Ps(10)
370 REAL Romp(10),Ro(10),Rb(10),CURRENT(10),Ns(10),MO(10),Rhs(10)
380 REAL CURRENT1(10),Ps1(10),Rhs1(10),Uoi(10,20),Ni(10,20),VOLT(5)
390 REAL Xmin,Xmax,Ymin,Ymax,F
400 DIM YTITLE$[60],TITLE$[60]
410 LET LAYER=0 ! Etching layer is zero.
420 DISP "DO YOU NEED A NEW ETCHING PROCESS?"
430 INPUT PROCESS$
440 DISP "ENTER NUMBER OF CURRENT FOR YOUR MEASUREMENTS!"
450 INPUT NUMBER ! Number of input current.
460 IF PROCESS$="N" OR PROCESS$="n" THEN 1710
470 FOR I=1 TO NUMBER
480    DISP "ENTER CURRENT VALUE IN THIS TIME!"
490    INPUT CURRENT(I)
500    IF CURRENT(I)=0 THEN 3250
510    FOR C=1 TO 2
520       FOR LOOP=1 TO 5
530          CLEAR 707
540          OUTPUT 707 :"VR7T1S11?"
550          TRIGGER 707
560          WAIT 1000
570          P=SPOLL (707)
580          IF P=68 THEN 600
590          GOTO 540
600          ENTER 707 ; VOLT(LOOP)
610       NEXT LOOP
620       VOL(C)=(VOLT(1)+VOLT(2)+VOLT(3)+VOLT(4)+VOLT(5))/5
```

```
630         DISP VOL(C)
640         IF C=2 THEN GOTO 720
650       BEEP
660         DISP "CHANGE CURRENT SOURCE POLARITY" ! Current source has two directi
ons.
670         INPUT OUTREAD$
680     NEXT C
690 !
700 !   A  verage resistance of two directions input current.
710 !
720     R(I)=ABS (VOL(1)-VOL(2))/(2*CURRENT(I))
730     IF R(I)<.0001 THEN I=I-1
740 NEXT I
750 BEEP
760 DISP "WHICH MEASUREMENT THIS IS?(VDP1, VDP2, HALL(0, 0.4))"
770 INPUT MEASURE$
780 IF MEASURE$="VDP1" THEN 790 ELSE 830
790 FOR J=1 TO NUMBER
800     Rmnop(J)=R(J)
810 NEXT J
820 GOTO 980
830 IF MEASURE$="VDP2" THEN 840 ELSE 880
840 FOR J=1 TO NUMBER
850     Romnp(J)=R(J)
860 NEXT J
870 GOTO 980
880 DISP "B=?"
890 INPUT FIELD
900 IF FIELD=0 THEN 920
910 GOTO 950
920 FOR J=1 TO NUMBER
930     Ro(J)=R(J)
940 NEXT J
950 FOR J=1 TO NUMBER
960     Rb(J)=R(J)
970 NEXT J
980 DISP "DO YOU NEED ANY OTHER MEASUREMENT?"
990 INPUT ANSWER$
1000 IF ANSWER$="Y" OR ANSWER$="y" THEN 470
1010 !
1020 ! Print result if Van Der Pauw measurement.
1030 !
1040 PRINT "VAN DER PAUW MEASUREMENT"
1050 PRINT "    "
1060 PRINT "Current(A)","Rmnop(Ohm)","ROmnp(Ohm)","Ps(Ohm/Square)"
1070 PRINT "----------","----------","----------","----------"
1080 FOR K=1 TO NUMBER
1090     IF Rmnop(K)<Romnp(K) THEN GOTO 1120
1100     FF=Rmnop(K)/Romnp(K)
1110    GOTO 1130
1120    FF=Romnp(K)/Rmnop(K)
1130    DISP "FF=",FF
1140    DISP "ENTER FACTOR VALUE?"
1150    INPUT F
1160     Ps(K)=4.53*F/2*(Rmnop(K)+Romnp(K))
1170     PRINT "   "
1180     PRINT CURRENT(K),Rmnop(K),Romnp(K),Ps(K)
1190 NEXT K
1200 !
1210 ! Print result of Hall Measurement on the printer.
1220 !
1230 DISP "NEXT PAGE PLEASE!"
1240 INPUT ANSWER$
```

```
1250 PRINT "HALL MEASUREMENT"
1260 PRINT " "
1270 PRINT "Current(A)","Delta R(OHM)","Rhs"
1280 PRINT "----------","------------","-------"
1290 FOR K=1 TO NUMBER
1300    DISP "HALL MEASUREMENT IS NORMAL?"
1310    INPUT ANSWER$
1320    IF ANSWER$="Y" OR ANSWER$="y" THEN 1350
1330    CHR(K)=ABS (Ro(K)+Rb(K))
1340    GOTO 1360
1350    CHR(K)=ABS (Ro(K)-Rb(K))
1360    Rhs(K)=CHR(K)/FIELD*10000
1370    PRINT " "
1380    PRINT CURRENT(K),CHR(K),Rhs(K)
1390 NEXT K
1400 DISP "WOULD YOU LIKE TO PRINT OUT THE RESULT?"
1410 PRINT "  "
1420 INPUT ANSWER$
1430 IF ANSWER$="N" OR ANSWER$="n" THEN 1570
1440 PRINT "RESULT"
1450 PRINT "          "
1460 PRINT "Current(A)","Ps(Ohm/Square)","Ns(cm-2)","Un(cm^2/v-s)"
1470 PRINT "---------","---------------","---------","-----------"
1480 FOR K=1 TO NUMBER
1490    Ns(K)=1/(Rhs(K)*1.6)*10^19 ! Calculate sheet concentration.
1500    MU(K)=10^19/(1.6*Ns(K)*Ps(K)) ! Calculate mobility
1510    PRINT "  "
1520    PRINT CURRENT(K),Ps(K),Ns(K),MU(K)
1530 NEXT K
1540 !
1550 ! Create Data File.
1560 !
1570 DISP "DATA FILE NAME?"
1580 INPUT DNAME$
1590 CREATE DNAME$&":D700",12,50
1600 ASSIGN# 1 TO  DNAME$&":D700"
1610 FOR K=1 TO NUMBER
1620    PRINT# 1 ; CURRENT(K),Ps(K),Rhs(K)
1630 NEXT K
1640 ASSIGN# 1 TO  *
1650 DISP "ETCHING PROCESS?"
1660 INPUT ETCHING$
1670 IF ETCHING$="Y" OR ETCHING$="y" THEN GOTO 440
1680 !
1690 ! Output The Data File.
1700 !
1710 DISP "RETRIEVED DATA FILE NAME?"
1720 INPUT DNAME$
1730 ASSIGN# 1 TO  DNAME$&":D700"
1740 FOR I=1 TO NUMBER
1750    READ# 1 : CURRENT(I),Ps(I),Rhs(I)
1760    DISP CURRENT(I),Ps(I),Rhs(I)
1770 NEXT I
1780 ASSIGN# 1 TO  *
1790 DISP "DO YOU WANT TO RETRIVE DATA AGAIN?"
1800 INPUT RETRIEVE$
1810 IF RETRIEVE$="Y" OR RETRIEVE$="y" THEN 1830
1820 GOTO 1900
1830 FOR I=1 TO NUMBER
1840    LET CURRENT1(I)=CURRENT(I)
1850    LET Ps1(I)=Ps(I)
1860    LET Rhs1(I)=Rhs(I)
```

```
1870     DISP CURRENT1(I),Ps(I),Rhs1(I)
1880 NEXT I
1890 GOTO 1710
1900 LAYER=LAYER+1
1910 DISP LAYER
1920 DISP "Enter each etching layer thickness please!"
1930 INPUT DEPTH
1940 LET A=.00000001*DEPTH
1950 FOR J=1 TO NUMBER
1960 !
1970 !  Depth Profile Calculation.
1980 !
1990 Uni(J,LAYER)=ABS ((Rhs(J)/Ps(J)^2-Rhs1(J)/Ps1(J)^2)/(1/Ps(J)-1/Ps1(J)))
2000 Ni(J,LAYER)=ABS ((1/Ps(J)-1/Ps1(J))/(1.6*(10^(-19))*A*Uni(J,LAYER)))
2010 NEXT J
2020 DISP "ARE YOU DONE?"
2030 INPUT DONE$
2040 IF DONE$="Y" OR DONE$="y" THEN 2060
2050 GOTO 1710
2060 DISP "Ploter is going to come!"
2070 FOR I=1 TO NUMBER
2080     PRINT "CURRENT IS",CURRENT(I),"(A)"
2090     PRINT "    "
2100     PRINT "LAYER","MOBILITY (CM2/S-V)","CARRIER CONCENTRATION (CM-3)"
2110     PRINT "------","--------------------","--------------------  ----------"
2120     FOR J=1 TO LAYER
2130         PRINT J,Uni(I,J),Ni(I,J)
2140     NEXT J
2150     PRINT "   "
2160 NEXT I
2170 DISP "WOULD YOU LIKE TO PLOT THE DATA ?"
2180 INPUT ANSWER$
2190 IF ANSWER$="N" OR ANSWER$="n" THEN 3250
2200 DISP "SCREEN(1) OR PLOTTER(2)?"
2210 INPUT ANSWER
2220 IF ANSWER=2 THEN 2340
2230 !
2240 ! Graph On The Screen
2250 !
2260 PLOTTER IS 1
2270 GCLEAR
2280 GRAPHALL
2290 ALPHA
2300 GOTO 2380
2310 !
2320 ! Graph On The Plotter.
2330 !
2340 PLOTTER IS 705
2350 OUTPUT 705 ;"VS8"
2360 DISP "SET UP PLOTTER AND PRESS END LINE"
2370 INPUT PRESS$
2380 DISP "INPUT Xmin,Xmax,LXmax,GXmax,Ymin,Ymax VALUES!"
2390 INPUT Xmin,Xmax,LXmax,GXmax,Ymin,Ymax
2400 Ymin=10^INT (LGT (Ymin))
2410 IF Ymax=10^INT (LGT (Ymax))<> 0 THEN Ymax=10^(INT (LGT (Ymax))+1)
2420 ! Draw X-axis and Y-axis
2430 LOCATE 20,120,15,85
2440 SCALE Xmin,GXmax,LGT (Ymin),LGT (Ymax)
2450 AXES GXmax/10,LGT (Ymax)-LGT (Ymin),Xmin,LGT (Ymin),1,1,2.5
2460 FOR I=0 TO LGT (Ymax)-LGT (Ymin)
2470     MOVE Xmin,LGT (Ymin)+I
2480     DRAW Xmin+(GXmax-Xmin)/70,LGT (Ymin)+I
```

```
2490     FOR J=2 TO 9
2500        MOVE Xmin.LGT (Ymin*J*10 I)
2510        DRAW Xmin+(GXmax-Xmin)/120.LGT (Ymin*J*10 I)
2520 ! Label X-axis
2530     NEXT J
2540 NEXT I
2550 CSIZE 2.5
2560 LDIR 0
2570 LORG 6
2580 I=0
2590 IF GXmax/10*I>GXmax THEN 2650
2600 MOVE GXmax/10*1,LGT (Ymin)-(LGT (Ymax)-LGT (Ymin))/100
2610 LABEL GXmax/10*I
2620 I=I+1
2630 GOTO 2590
2640 ! Label Y-axis
2650 LDIR 0
2660 LORG 8
2670 FOR I=0 TO LGT (Ymax)-LGT (Ymin)
2680     MOVE -(GXmax/250).LGT (Ymin*10^I)
2690     LABEL 10^(LGT (Ymin)+I)
2700 NEXT I
2710 DISP "WHICH CURRENT VALUE YOU WANT TO PLOT FOR PROFILE?"
2720 DISP "GIVE INTEGE NUMBER (1 TO CURRENT NUMBER)"
2730 INPUT I
2740 LET D=0
2750 DISP "WHICH PLOTTER DO YOU WANT?(PRESS M OR C)"
2760 INPUT ANSWER$
2770 DISP "PLOTTER TITLE?"
2780 INPUT TITLE$
2790 IF ANSWER$="C" OR ANSWER$="c" THEN 2080
2800 FOR J=1 TO Xmax/DEPTH
2810     LET D=DEPTH+D
2820     MOVE D.LGT (Uni(I.J))
2830     LABEL "*"
2840 NEXT J
2850 YTITLE$="Mobility (cm2/v-s)"
2860 ! Carrier concentration plotter.
2870 GOTO 3060
2880 FOR J=1 TO Xmax/DEPTH
2890     LET D=D+DEPTH
2900     MOVE D.LGT (Ni(I,J))
2910     LABEL "*"
2920 NEXT J
2930 DISP "PROJECTED RANGE, DEVIATION, DOSE? (CM)"
2940 INPUT Rp,De,Qo
2950 LET A=0
2960 LET B=Qo/(6.28^.5*De)*EXP (-(.5*(Rp/De)^2))
2965 PRINT B
2970 MOVE A.B
2980 WHERE A.B
2990 FOR J=0 TO LXmax STEP 10
3000     LET N=Qo/(6.28^.5*De)*EXP (-(.5*((J*.00000001-Rp)/De)^2))
3010     IF N<Ymin THEN DRAW J.LGT (Ymin)
3020     DRAW J.LGT (N)
3030 NEXT J
3040 YTITLE$="Carrier Concentration (CM-3)"
3050 ! Label plotter title!
3060 LORG 6
3070 CSIZE 4..6.10
3080 MOVE (GXmax-Xmin)/2,LGT (Ymax)+(LGT (Ymax)-LGT (Ymin))/10
3090 LABEL TITLE$
3100 ! Label X-axis title!
```

```
3200 LABEL YTITLE$
3210 WAIT 20000
3220 DISP "DO YOU WANT TO PLOT AGAIN?"
3230 INPUT ANSWER$
3240 IF ANSWER$="Y" THEN 2170
3250 END
```

```
10 ! ************************************************************************
20 !
30 ! Program Title: RAMPING
40 !
50 ! Programmer    : Yanan Shieh
60 !
70 ! Date          : 12-11-88
80 !
90 ! Version       : 1.0
100 !
110 ! Description : This program controls temperature controller to ramp
120 !                 temperature either upwards or downwards in temperature:
130 !                 it also controls keithley and fluke DVMS to record
140 !                 two voltages, one is from thermocouple (keithley
150 !                 reading)which is converted to temperature in celsius.
160 !                 other is from output voltage of boxcar which is PIIS
170 !                 signal.
180 !
190 !
200 ! ************************************************************************
210 OPTION BASE 1
220 CLEAR
230 DIM F$[16],I$[50]
240 REAL TEMPR(500,2),TEMPV(500,2)
250 REM HEATER POWER,GAIN,RATE ARE RESET ARE SET MANUALLY BY THE
260 REM USER. THE INITIAL SETPOINT TEMPERATURE IS ENTERED VIA THE
270 REM KEYBOARD. THE TIME IN SECONDS AND DESIRED FINAL TEMPERATURE
280 REM ARE REQUESTED. THE 81C WILL RAMP THE SET POINT TO THE FINAL
290 REM TEMPERATURE LINEARLY WITH A QUANTIZED TEMPERATURE INCREMENT
300 REM 0.1K FOR NORMAL RAMP SPEEDS.
310 DIM A$[50] ! Dimention array for reading the DRC 81C
320 T_WAIT=20 ! Sampling rate in seconds
330 K_EQB=.9 ! Incremental change in control T which implies equilibrium
340 CLEAR ! Clear the display
350 REM REQUEST THE INITIAL SETPOINT TEMPERATURE.
360 DISP "INITIAL TEMPERATURE :";@ INPUT K_INITIAL
370 BEGIN: DISP "SELECT A HEATER POWER,GAIN,RATE AND RESET MANUALLY"
380     DISP "ON THE DRC-81C TO OBTIAN THE DESIRED INITIAL TEMPERATURE."
390     DISP
400     DISP "TEMPERATURE TO RAMP TO":@ INPUT K_FINAL
410     DISP "TIME TO REACH ";K_FINAL;" K";" IN SECONDS":@ INPUT T_FINAL
420     DISP "INCREMENT OF TEMPERATURE TO TAKE DATA." @ INPUT K_INC
430 REM ADJUST THE DRC 81C TO OBTIAN EQUILIBRIUM AT THE INITIAL SETPOINT.
440     OUTPUT 712 ;"S";VAL$ (K_INITIAL)
450     K=K_INITIAL
460     WAIT1: WAIT 1000*T_WAIT ! WIAT T_WAIT SECONDS
470         K0=K
480         OUTPUT 712 ;"RC" @ ENTER 712 ; A$ ! READ CONTROL TEMPERATURE.
490         K=VAL (A$[1,6])
500         IF ABS (K-K0)>K_EQB OR ABS (K-K_INITIAL)>1 THEN WAIT1
510     OUTPUT 712 ;"R1" @ ENTER 712 ; A$ ! READ R1
520     DISP "R1 =";A$
530 POSITION=VAL (A$[1])
540 DISPLAY_ID$=A$[3,5]
550 CONTROL_ID$=A$[7,9]
560 GAIN=VAL (A$[11,12])
570 RATE=VAL (A$[14,15])
580 RESET1=VAL (A$[17,18])
590 HEATER_RANGE=VAL (A$[20])
600   PRINTER IS 701
610 PRINT "REMOTE SENSOR POSITION=";POSITION
620 PRINT "DISPLAY SENSOR ID=";DISPLAY_ID$
```

```
630 PRINT "CONTROL SENSOR ID=";CONTROL_ID$
640 PRINT "GAIN=";GAIN,"RATE=";RATE,"RESET=";RESET1
650 PRINT "HEATER POWER RANGE=";HEATER_RANGE;"WATTS"
660 P=1
670 T=0
680 K_SPINC=.1 ! NORMAL INCREMENT OF SETPOINT
690 SETPOINT=K_INITIAL
700 SLOPE=(K_FINAL-K_INITIAL)/T_FINAL ! COMPUTER RAMP SLOPE(K/SEC.)
710 DISP "RAMP = ";60*SLOPE;"KELVIN PER MINUTE";"KELVIN PER SECOND"
720 T_INC=K_SPINC/ABS (SLOPE) ! TIME TO INCREMENT SETPOINT IN SECOND
730 IF T_INC<.9 THEN K_SPINC=.2 @ T_INC=2*T_INC
740 IF T_INC<1 AND K_SPINC=.2 THEN T_INC=2.5*T_INC @ K_SPINC=.5
750 ON TIMER# 1.1000*T_INC GOTO GO  ! TIMEOUT T_INC SECONDS - RESTART TIMER
760    PROCEED: GOTO PROCEED  ! YES THIS STATEMENT IS CORRECT
770    GO: OUTPUT 712 :"WC" @ ENTER 712 ; A$ ! 80 MS READ TIME.
780    IF ER (ABS (SETPOINT-K_INITIAL)/K_INC)>0 THEN SKIP
790    DISP T;" SECONDS : ";"SETPOINT = ";SETPOINT;" K"
800    DISP "CONTROL TEMPERATURE =";A$ ! ALL DISP TAKE .23SECONDS
810 ! Select a temp. range to optimize the gain.
820 IF SETPOINT=94 THEN 1490
830 IF SETPOINT=114 THEN 1520
840 IF SETPOINT=138 THEN 1550
850 IF SETPOINT=162 THEN 1580
860 IF SETPOINT=186 THEN 1610
870 IF SETPOINT=208 THEN 1640
880 IF SETPOINT=232 THEN 1670
890 IF SETPOINT=256 THEN 1700
900 IF SETPOINT=280 THEN 1730
910 IF SETPOINT=304 THEN 1760
920 IF SETPOINT=328 THEN 1790
930   PRINT "SET";SETPOINT,"CONL.";A$
940    TEMPR(P,1)=VAL (A$)
950    TEMPR(P,2)=T
960    TEMPV(P,1)=SETPOINT
970  ! READS FLUKE DVM
980    OUTPUT 707 :"VR7D8T1?" @ ENTER 707 : F$
990    MANTISSAF$=F$[1,8] @ EXPONENTF$=F$[10,12]
1000    TEMPV(P,2)=VAL (MANTISSAF$)*10^VAL (EXPONENTF$)
1010    PRINT "PITS=",TEMPV(P,2)
1020    DISP USING 1030 : P,TEMPR(P,1),TEMPV(P,2)
1030   IMAGE "READING NUMBER",2X,DDD,4X,"THERMAL COUPLE TEMP.",2X,DDDD.DDD,2X,"V
OLTAGE",2X,DDDD.DDDDD
1040 P=P+1
1050    SKIP: T=T+T_INC ! ADD TIME FOR T_SPINC
1060    IF T>T_FINAL THEN COMPLETE ! IS RAMP TIME PERIOD COMPLETE?
1070    SETPOINT=SETPOINT+K_SPINC*SGN (SLOPE) ! INCREMENT THE SETPOINT
1080    OUTPUT 712 :"S";VAL$ (SETPOINT)
1090 GOTO PROCEED
1100 COMPLETE: DISP "RAMPING COMPLETE." @ OFF TIMER# 1
1110 K_INITIAL=K_FINAL
1120 FOR J=10 TO 160 STEP 50 @ BEEP J,500 @ NEXT J
1130 ON ERROR GOTO 1250
1140 ! Store_data:
1150 DISP "ENTER THE PITS FILE NAME!" @ INPUT file_name$
1160 DISP "NUMBER OF READINGS =";P-1
1170 CREATE file_name$&":D700",400,20
1180 ASSIGN# 1 TO  file_name$&":D700"
1190 FOR N=1 TO P-1
1200 PRINT# 1 ; TEMPV(N,1),TEMPV(N,2)
1210 NEXT N
1220 ASSIGN# 1 TO  *
1230 DISP "READING COMPLETE!"
1240 GOTO 1300
```

```
1250 OFF ERROR
1260 BEEP 50,500
1270 DISP "FILE NAME ERROR.TRY A DIFFERENT FILE NAME!"
1280 WAIT 4000
1290 GOTO 1140
1300 DISP "NEED TO STORE RAMPING DATA?" @ INPUT ANS$
1310 IF ANS$="N" THEN 1820
1320 DISP "RAMPING NUMBER=";P-1
1330 ON ERROR GOTO 1420
1340 DISP "ENTER RAMPING DATA FILE NAME" @ INPUT ramp_name$
1350 CREATE ramp_name$&":D700",400,20
1360 ASSIGN# 2 TO  ramp_name$&":D700"
1370 FOR M=1 TO P-1
1380 PRINT# 2 ; TEMPR(M,2),TEMPR(M,1)
1390 GOTO 1460
1400 ASSIGN# 2 TO  *
1410 NEXT M
1420 OFF ERROR @ BEEP 50,500
1430 DISP "FILE NAME ERROR. TRY DIFFERENT FILE NAME!"
1440 WAIT 4000
1450 GOTO 1340
1460 DISP "READING COMPLETE!"
1470 GOTO 1820
1480 ! Change the gain.
1490 OUTPUT 712 ;"P";93;"W1" @ ENTER 712 ; K1
1500 DISP K$ @ PRINT K$
1510 GOTO 930
1520 OUTPUT 712 ;"P";90;"W1" @ ENTER 712 ; K$
1530 DISP K$ @ PRINT K$
1540 GOTO 930
1550 OUTPUT 712 ;"P";84;"W1" @ ENTER 712 ; K$
1560 DISP K$ @ PRINT K$
1570 GOTO 930
1580 OUTPUT 712 ;"P";80;"W1" @ ENTER 712 ; K$
1590 DISP K$ @ PRINT K$
1600 GOTO 930
1610 OUTPUT 712 ;"P";76;"W1" @ ENTER 712 ; K$
1620 DISP K$ @ PRINT K$
1630 GOTO 930
1640 OUTPUT 712 ;"P";80;"W1" @ ENTER 712 ; K$
1650 DISP K$ @ PRINT K$
1660 GOTO 930
1670 OUTPUT 712 ;"P";84;"W1" @ ENTER 712 ; K$
1680 DISP K$ @ PRINT K$
1690 GOTO 930
1700 OUTPUT 712 ;"P";90;"W1" @ ENTER 712 ; K$
1710 DISP K$ @ PRINT K$
1720 GOTO 930
1730 OUTPUT 712 ;"P";94;"W1" @ ENTER 712 ; K$
1740 DISP K$ @ PRINT K$
1750 GOTO 930
1760 OUTPUT 712 ;"P";96;"W1" @ ENTER 712 ; K$
1770 DISP K$ @ PRINT K$
1780 GOTO 930
1790 OUTPUT 712 ;"P";98;"W1" @ ENTER 712 ; K$
1800 DISP K$ @ PRINT K$
1810 GOTO 930
1820 END
```

PULSED LASER ANNEALING AND CHARACTERIZATION OF GaAs SUBSTRATES

by

YANAN F. SHIEH

B.S., Shanghai University, 1984
Shanghai, P. R. China

AN ABSTRACT OF A MASTER'S THESIS

submitted in partial fulfillment of the

requirements for the degree

MASTER OF SCIENCE

Department of Electrical and Computer Engineering

KANSAS STATE UNIVERSITY
Manhattan, Kansas

1989

ABSTRACT

Pulsed laser annealing using, a rare halide excimer laser (λ = 308 nm) with 12 nsec pulse duration and with energy densities from 0.2 to 0.32 J/cm^2, was performed on commercial semi-insulating gallium arsenide substrates which were ion implanted with Se or Si ion doses ranging from $2x10^{12}$ to $6x10^{14}$ cm^{-2}. The residual defects in annealed GaAs samples were investigated by means of photo-induced transient spectroscopy (PITS) which is based on an observation of the emission coefficient behavior associated with deep level traps following an incident trap-filling light pulse. The PITS system includes a 10 mW He-Ne laser, an optical chopper, a boxcar integrator, and a close-cycle helium refrigerator.

Three dominant and one trace peaks were observed in the PITS spectra (from 40K to 380K) which correspond to the activation energies of deep levels from 0.02 eV to 0.8 eV. The effectiveness of pulsed laser annealing for restoring the electrical properties such as charge carrier activation and the electron mobility was examined by using the Hall effect and van der Pauw measurements. Although the layer recrystallization was good (as inferred from the Raman spectra) and the sheet carrier concentration was high, the electron mobility was low. An attempt to

correlate the concentration of implanted impurities with the charge carrier and deep level defect densities was made. Extensive comparisons of over all characteristics of pulsed laser annealed samples with conventional furnace annealed samples were also presented.